TRAJECTORIES OF GROUP AND INDIVIDUAL-LEVEL STRUCTURAL BRAIN NETWORK ORGANIZATION FROM BIRTH TO CHILDHOOD AND THEIR COGNITIVE RELEVANCE

Mackenzie A. Woodburn

A thesis submitted to the faculty at the University of North Carolina at Chapel Hill in partial fulfillment of the requirements for the degree of Master of Arts in the Psychology & Neuroscience Department.

Chapel Hill
2020

Approved By:

Jessica R. Cohen

Margaret A. Sheridan

Kelly Giovanello

ABSTRACT

Mackenzie Woodburn: Trajectories of group and individual-level structural brain network organization from birth to childhood and their cognitive relevance
(Under the direction of Jessica R. Cohen)

Brain networks are theorized to become more segregated to support early cognitive specialization, and then later increase integration between networks to support more complex cognition across development. The present study examined the organization of structural brain networks derived from cortical thickness during infancy to childhood in a longitudinal sample (0-6 years). On the group level, we observed a shift towards increasing network segregation at the second year of life, and a later shift towards network integration at year six. This study also related subject-based maturational coupling across different developmental timeframes to cognitive outcomes at 7-10 years. Protracted integration of maturational coupling throughout infancy into middle childhood (0-6 years) was correlated with working memory performance in later childhood (7-10 years). These results support the model that describes early increasing segregation followed by later integration, and demonstrate that integrated structural maturation from infancy to childhood supports higher order cognition like working memory.

TABLE OF CONTENTS

LIST OF TABLES

LIST OF FIGURES

LIST OF ABBREVIATIONS

ANOVA	Analysis of variance
DAS	Differential Ability Scale
DK	Desikan-Killiany
DWI	Diffusion-weighted Image
EF	Executive Functions
FA	Fractional Anisotropy
GCA	General Conceptual Ability
HAMMER	Hierarchical Attribute Matching Mechanism for Elastic Registration
MCN	Maturational Covariance Network
MRI	Magnetic Resonance Imaging
PC	Participation coefficient
sbMCN	subject-based Maturational Coupling Network
SCN	Structural Covariance Network
SES	Socioeconomic Status
SRT	Serial Reaction Time
TR	Repetition Time
TE	Echo Time
UNC	University of North Carolina

INTRODUCTION

Brain maturation is a complex process that occurs at different rates for different areas of cortex. For example, maturity as determined by cortical growth is first achieved in sensory cortex, followed by association cortex such as parietal and frontal regions (Huttenlocher, 1990). Cognitive development follows a similar trajectory: children first develop basic sensory and perceptual abilities, which are followed by the gradual emergence of more complex cognition, such as executive functions (EF) – a set of higher order skills needed for goal-oriented behavior (Johnson, 2011; Best & Miller, 2010). A traditional maturational framework of brain development has broadly described the emergence of cognitive abilities as reliant on the maturation of a functionally related brain region (for a review, see: Johnson, 2001). However, the brain is highly interconnected, and recent literature has begun to characterize the maturation of interactions across brain regions at the network level (Cao et al., 2017; Grayson & Fair, 2017; Morgan et al., 2018; Zhao et al., 2019). The interactions across brain regions at the network level likely provides the infrastructure necessary for cognition to emerge (for a review, see: Johnson, 2011).

Specialization and integration are general processes that have been used to describe emergent cognition from infancy into childhood (Johnson & Munakata, 2005). Fundamental work across several cognitive domains (e.g. perception, language, executive functions) has revealed strong evidence of specialization, or dissociable cognitive processing, early in development (for reviews, see Johnson 2001; Johnson & Munakata, 2005). It has been proposed

that specialization allows for more efficient cognition, such that older children process information more selectively and more quickly than younger children (Johnson, 2000). After early cognitive specialization, it is thought that cognition then becomes increasingly more integrative across distinct cognitive domains. This pattern of increased specialization, followed by increased integration, is evident for both sensorimotor processes and executive functions, albeit on different timeframes (e.g. the first years of life for sensorimotor development and protracted EF development; D'Souza et al., 2017; Luna et al., 2015) . Johnson and Munakata (2005) argue that increased specialization reduces computational redundancy to provide complementary processes that eventually can be integrated to allow for more complex cognition, which is ultimately why cognitive specialization and integration are important processes for cognitive development.

Cognitive specialization and integration putatively map onto changes shown in brain function and structure (Johnson & Munakata, 2005; Luna et al., 2015). Recent application of graph theory network analyses to brain function and structure have supported this brain-behavior correspondence (Baum et al., 2017; Marek et al., 2015). Graph theory metrics can quantify the way brain networks *segregate* – form strong local connections within networks, which may support cognitive specialization. Graph metrics can also quantify the way brain networks *integrate* - form long-range connections that span discrete brain networks, which may support cognitive integration (Sporns, 2013). Though neither graph theory nor infant neuroimaging are exactly new in practice, the combination of the two is still in its infancy (for reviews see: Cao et al., 2017; Grayson & Fair, 2017; Morgan et al., 2018; Zhao et al., 2019). Within the past few years, a surge of studies has investigated the organization of brain networks from infancy to childhood (Gao et al., 2011; Gao et al., 2014; Gao et al., 2015; for reviews, see: Cao et al., 2017;

Zhao et al., 2019). Literature investigating the organization of brain networks from infancy to childhood has shown that functional connections within networks become increasingly synchronized and strengthened during the first year of life, and stabilize into year two (Gao et al., 2011). Additionally, while the number of functional connections between these networks decreases during the first two years of life, the remaining inter-network connections become stronger (Gao et al., 2011, Gao et al., 2014). In other words, early brain networks become more internally coherent and segregated and later become more integrated — similar to the pattern of earlier increased specialization and later increased integration of cognitive processes.

Structural covariance and maturational coupling during childhood

Brain networks derived from cortical thickness demonstrate how brain structure is organized, which is thought to be the result of how brain structure has matured. Several types of networks derived from cortical thickness exist (Figure 1). Structural covariance networks are obtained by correlating regional cortical thickness of pairs of regions across subjects (for a review, see: Alexander-Bloch, Giedd, & Bullmore, 2013). Thus, they measure how cortical regions covary in thickness on a group level. Networks derived from structural covariance are nearly identical to networks derived from functional connectivity measures in adulthood, suggesting that cortical thickness may also relate to cognition as has been shown with brain function (Alexander-Bloch et al., 2013; Smith et al., 2019). Maturational covariance has been shown to recapitulate network organization of structural covariance, which suggests that groups of regions that have similar cortical thickness across subjects likely matured similarly across subjects over the course of development (Alexander-Bloch et al., 2013).

Brain network changes in integration and segregation across early development have been reported by the few studies using structural covariance of cortical thickness across early

developmental. One such study by Fan and colleagues examined structural covariance from a longitudinal cohort who were scanned using structural MRI at birth, 1 year, and 2 years (Fan et al., 2011). A small-world topology of brain networks was present at birth, meaning that dense clusters of local connections with sparser, long-range connections across clusters were detected. Both network segregation and network integration increased across time similarly. This same trajectory of increasing integration and segregation was supported by another study with the same cohort using structural networks derived by cortical folding and fiber density (Nie et al., 2014). Two similar studies examined structural covariance via cortical thickness in two different cross-sectional cohorts between the ages of 3 to 20 years (Nie et al., 2013; Khundrakpam et al., 2012). Both reported initial increases in segregation from early childhood that transitioned into a gradual decrease in segregation during middle childhood, which began to increase again during adolescence. The opposite relationship was found with structural network integration during this timeframe. Initial decreases in integration were found during early childhood, which then switched to increases in integration during middle childhood that either stabilized or slightly decreased during adolescence. The results of these studies of structural covariance suggest there is a developmental balance between structural network integration and segregation, and that the time of early childhood is characterized by a shift towards increasing segregation, and then a later shift towards increasing integration.

No cognitive measures have been related to structural covariance organization early in development. However, the cognitive relevance of these changes in structural network organization have been indicated later in development with another study by Khundrakpam and colleagues (2017). Structural covariance organization in children and adolescents with higher intelligence quotients was both more segregated and more integrated compared to those with

lower intelligence quotients. This finding in the modality of brain structure appears to be consistent with functional neuroimaging studies that have found more specific relationships between network organization and cognition (Bassett et al., 2013, Bassett et al., 2015; Cohen & D'Esposito, 2016; for reviews, see: Shine & Poldrack, 2018; Cohen, 2018). For example, functional brain networks demonstrate greater integration during complex working memory tasks like the n-back task that engage multiple cognitive systems, such as attention, memory, and cognitive control (Cohen & D'Esposito, 2016, Finc et al., 2017). During tasks that engage single cognitive systems, such as a motor execution task, greater segregation is observed (Cohen & D'Esposito, 2016). More research has been done in functional neuroimaging to find that different patterns of network organization support different cognitive processes. More research is needed in structural neuroimaging to characterize maturational trajectories during early development and determine if these trajectories are related to cognition.

Traditionally, cortical thickness networks are measured at the group level, but subject level analysis of how brain regions have similar maturational trajectories, or maturational coupling, has been recently introduced (Khundrakpam et al., 2019). Using the subject-based maturational coupling network (sbMCN) approach, the similarity of cortical thickness trajectories across time between any two regions can be assessed on the individual level by calculating a maturational coupling index for subsequent network analysis as sbMCNs (See Figure 1c). In a developmental sample between 5 to 25 years acquired with an accelerated longitudinal design, regions with similar maturational trajectories within a subject also had similar structural covariance at the group level. This result suggests that regions that mature similarly lead to similar levels of cortical thickness. No study has yet to quantify sbMCNs across early development, nor assessed how sbMCNs relate to cognitive outcomes.

In summary, the relevance of structural brain network development to cognitive development is still unclear and is the ultimate goal of the current study. Previous literature reviews describing processes of change in cognitive and brain development (Cao et al., 2017; Johnson & Munakata, 2005; Luna et al., 2015) theorize that increased segregation and integration support cognitive development based on empirical work that covers age ranges of infancy and childhood separately, not together. Structural brain network organization from birth to childhood has yet to be examined in a single study to test this model of development. The current study leveraged the strengths of an existing longitudinal neuroimaging dataset to answer questions related to the developmental process of cortical network maturation on the group level, as well as how individual variation in cortical network maturation relates to cognitive outcomes assessed at 7-10 years. Previous research has documented earlier motor specialization and protracted development of higher order cognition like working memory (D'Souza et al., 2017; Best & Miller, 2010), which may map onto trajectories of early increases in segregation, and later increases in integration. Given this evidence, we hypothesized that earlier segregated maturation during infancy would be related to motor learning performance, and that protracted integration would be related to working memory performance.

METHODS

Participants

The Institutional Review Board of the University of North Carolina (UNC) School of Medicine approved this study. Pregnant mothers were recruited during their second trimester of pregnancy from the UNC hospitals registry. Informed consent was obtained from both parents. Exclusion criteria included prenatal or congenital anomalies, or presence of any major medical or

mental illness in the mother. Initially, 93 healthy infants were recruited to undergo a longitudinal MR imaging study of early brain development, but a total of 50 subjects (24 females) were used for analysis of this study based on criteria of having at least three timepoints of good quality data (see Image Processing section for operationalization of good quality data).

All participants of this longitudinal study are currently being contacted to return for an additional timepoint between the ages 7 to 10 years old. Thus far, 32 participants have returned for the 7-10 year timepoint (mean age = 9.31, SD = 0.49, minimum age = 7.4, maximum age = 10.5, 18 females). While initial inclusion criteria included typical development, when assessed at ages 7-10, five subjects were diagnosed with a developmental disorder (Attention Deficit Hyperactive Disorder [n=3] Autism Spectrum Disorder [n=1], or developmentally delayed [n=1]). Measures of socioeconomic status (SES) such as household income and maternal education were not significantly correlated with the number of timepoints for each subject (household income: $r = 0.138$, $p = 0.465$; maternal education: $r = 0.171$, $p = 0.346$).

Study Procedure

Study sessions occurred every 3 months between 2 weeks to 12 months (0, 3, 6, 9, 12 months), at 18 months, and then annually between 2 and 6 years. This resulted in a total of 11 possible time points (i.e. 0, 3, 6, 9, 12, 18, 24, 36, 48, 60, and 72 months). Not all subjects participated in all time points due to participant dropout or unavailability when scheduling a visit. The distribution of existing subject time points are illustrated in Figure 2. The mean number of timepoints per subject was 6.76 (range: 3-11). All subjects were imaged during natural sleep without the use of sedation when they were infants and toddlers (ages 0-2). The protocol for conducting asleep scans was similar to recommendations for infant neuroimaging

studies (Dean et al., 2014). When subjects returned for later time points at age three and beyond, subjects underwent scans asleep or awake, but awake status was not recorded consistently from subject to subject. During awake scans, subjects watched a movie of their choice inside the MRI scanner.

Behavioral Measures

A subset of 31 subjects who returned for their visits at the ages of five or six were assessed on general cognitive performance using the upper level Early Years Battery of the Differential Ability Scales - Second Edition (DAS-II; Elliott, 2007). The DAS-II is a standardized cognitive assessment that evaluates a variety of cognitive domains for both typically and atypically developing children between 2.5 to 18 years of age. The upper level Early Years Battery specifically assesses children between the ages of 3.5 to 7 years. The upper level Early Years Battery of the DAS-II contains six core subtests that measure verbal reasoning (Verbal Comprehension and Naming Vocabulary), non-verbal reasoning (Picture Similarities and Matrices), and spatial ability (Pattern Construction and Copying). Scores on these six subtests are combined to produce the general conceptual ability (GCA) score.

All subjects who returned between the ages of 7-10 completed four fMRI tasks and neuropsychological assessment. This manuscript focuses on two well-established block design fMRI tasks successfully used with children 7-10 years old that evaluate motor learning (serial reaction time task) and working memory (n-back task). These tasks are theoretically relevant to assess motor and EF development, respectively.

For the Serial Reaction Time (SRT) task, participants were told to indicate the location of an ‘X’ presented on the screen by a button press (Figure 3). Participants who were left-handed were not excluded from this task (N=3), and were asked to use their right hand during the task.

There were two conditions in this task: 1) a sequence condition, which consisted of a repeating 12-item pattern (i.e. 1-2-3-1-4-3-4-2-1-3-2-4); and 2) a random condition, which consisted of a pseudorandom order. The pseudorandom order was constrained such that items could not be a repeat of a previous trial, nor could a random block begin or end with the same item that the sequence block started or ended. For each trial, the letter 'X' was presented for 1 second with an inter-stimulus interval of 250 milliseconds. This trial timing is consistent with prior work (Cohen & Poldrack, 2008) and has been successfully administered to children of this age range (Thomas et al., 2004). Each block contained 24 trials. Each run contained 4 blocks each of sequence and random conditions in an interleaved order for a total of 8 blocks. A 24 second crosshair was presented at the start and end of a run, and between every 4 blocks. Across participants, the interleaved order of the SRT was counterbalanced. Two runs of 5.2 minutes each of the SRT task were collected. The SRT probes motor sequence learning such that participants become faster on sequence trials as compared to random trials with practice (Cohen & Poldrack, 2008, Robertson, 2007, Thomas et al., 2004). Response times, as well as the response time differences between random and sequence conditions from run to run, were used as measures of motor learning for this study. Inverse efficiency was also used as a measures of motor learning, which is the response time in milliseconds divided by the accuracy to responded trials. Neurally, the SRT recruits motor learning circuitry (basal ganglia, premotor and motor cortices, and parietal cortex) and is broadly supported by increasingly segregated brain networks as sequences become learned (Bassett et al., 2015; Lin et al., 2016; Miraglia et al., 2018).

For the n-back task, participants were told to respond with a button press whether the current stimulus was the same as (a 'match') or different from (a 'non-match') the stimulus seen n previously (Figure 4). The n-back task evaluates a type of executive function known as

working memory, which is the ability to encode, maintain, and update relevant information (Baddeley, 1992). 0- and 2-back conditions of the n-back task were administered to examine low and high working memory load conditions respectively. For the 0-back condition, 'X' was used as a 'match' and any other letter was a 'non-match'. For the 2-back condition, participants responded whether the current stimulus was a 'match' or a 'non-match' to the letter presented two previously. For each trial, a letter stimulus was presented for 1 second with an inter-stimulus interval of 1 second. Each block contained 20 trials that included 4 match trials and 16 non-match trials. There were 5 null event trials lasting 2 seconds each randomly interspersed throughout each block. A 10 second crosshair was presented at the start of a run. Then each task block began with a 6-second presentation of either 'Not X or X' or 'No Match or Match' for 0- and 2-back blocks, with jittered intervals in between trials and at the end of trials that lasted 2-4 seconds. Rest blocks between two task blocks consisted of a 6-second presentation of 'REST' and 24 seconds of crosshair presentation. Each run contained four blocks (two each of 0- and 2-back conditions) in a randomized order for a total of 5.2 minutes. Two runs of the n-back task were acquired from each subject. Several studies have demonstrated the ability of children 7-10 years old to successfully complete the n-back task (Cieselski et al., 2006; Roussotte et al., 2011; Schleepen et al., 2009; Stollstorff et al., 2010). Accuracy on 2-back target trials and d' were used as measures of n-back performance. D' was calculated as the difference between z-transformed hit rate and z-transformed false alarm rate, and is a measure of signal detection.

Image Acquisition

For each time point in this study, T1, T2, and diffusion-weighted (DWI) images were acquired using a 3T Siemens scanner (TIM TRIO until 2016; PRISMA after 2016) with a 32-channel head coil. All three types of structural brain images were acquired for optimal distinction

of gray and white matter throughout infancy and early childhood. The tissue boundaries during this age range are not as clear when using intensity-based segmentation and thus all three of these structural images are needed for optimal processing (Shi et al., 2010). T1 images (144 sagittal slices) were acquired with the following parameters: repetition time (TR) = 1,900 ms, echo time (TE) = 4.38 ms, flip angle = 7, acquisition matrix = 256 × 192, and voxel size = 1 × 1 × 1 mm^3. T2 images (64 axial slices) were acquired with the following parameters: TR = 7,380 ms, TE = 119 ms, flip angle = 150, acquisition matrix = 256 × 128, and voxel size = 1.25 × 1.25 × 1.95 mm^3. Diffusion-weighted images (DWI) (60 axial slices) were acquired with the following parameters: TR = 7,680 ms, TE = 82 ms, acquisition matrix = 128 × 96, voxel size = 2 × 2 × 2 mm^3, 42 non-collinear diffusion gradients, and diffusion weighting b =1000s/mm^2. Resting-state fMRI scans were additionally collected in a subset of participants, but will not be discussed here.

Image Processing & Cortical Surface Construction

Structural brain images were processed with an imaging pipeline validated for cortical surface analysis that is specific to and optimized for longitudinal infant MRI scans (for a review, see: Li et al., 2018; see Figure 5 for a flowchart of this pipeline). In this pipeline, the T2 image and the fractional anisotropy (FA) image derived from the DWI scan were aligned onto the T1 image for each subject and then resampled to single millimeter cubic space using FSL's FLIRT function (Smith et al., 2004). Aligned images were then skull-stripped using a learning-based meta-algorithm (Shi et al., 2012). The HAMMER (Hierarchical Attribute Matching Mechanism for Elastic Registration) method was used to remove the brainstem and cerebellum (Shen & Davatzikos, 2002). Next, the nonparametric nonuniform intensity normalization (N3) method was used to correct image intensity inhomogeneities before rigid alignment of each subject's longitudinal images (Sled et al., 1998). Multi-modal structural brain images were then segmented

using an infant-specific 4D multi-modal segmentation method (Wang et al., 2012). Non-cortical surfaces were masked and filled before the left and right hemispheres were separated. To correct topological defects that occur when segmenting infant brain images, a topologically-preserving surface method was utilized (Li et al., 2014a). This topological correction preserves the initial topology of the cortical surface while smoothing the surface to reconstruct the inner and outer cortical surfaces. The inner cortical surface was then mapped onto the spherical space of FreeSurfer (Fischl, 2012). The Spherical Demons registration method was used for intra- and inter-subject registration (Yeo et al., 2010). See Li et al. (2014b) for more details on infant registration. Images that did not pass quality control inspection throughout steps of this pipeline were considered poor quality, which resulted in 50 subjects with at least three timepoints for subsequent analyses.

Sulcal-gyral based parcellation was then applied using an automated labeling system to divide the cortical surface into 64 cortical regions using the Desikan-Killiany (DK) Atlas (Desikan et al., 2006). Additional analyses using a larger number of 148 cortical regions with the Destrieux Atlas were also conducted to replicate results of the DK atlas (Destrieux et al., 2010). Finally, cortical thickness was measured by taking the minimum distance between the reconstructed inner and outer cortical surfaces at each vertex of space. Each region's cortical thickness was computed by averaging the cortical thickness for all vertices included in that region.

Structural Covariance Networks

From the longitudinal sample, each of the 11 time points were considered separately for group level analyses. For each time point, correlation matrices were constructed based on the across-subject correlations of cortical thickness between all pairs of regions. Each cortical region

was defined as a node, and correlations of cortical thickness between all pairs of regions were defined as edges. Similar to previous work (Nie et al., 2014; Khundrakpam et al., 2017), linear regression was used to remove effects of sex and mean overall cortical thickness, and the remaining residuals were used to calculate across-subject correlations between each pair of brain regions for each time point. This resulted in a 64 x 64 correlation matrix for the DK atlas, and 148 x 148 correlation matrix for the Destrieux atlas for each time point. Each region of interest (ROI) in the correlation matrix was grouped and arranged by the 7 networks defined by Yeo and colleagues (Yeo et al., 2011; see Figure 6). These 7 networks include the visual, somatomotor, dorsal attention, ventral attention, limbic, frontoparietal, and default networks.

The graph theoretical metrics used for this study include metrics that measure network segregation and integration respectively, specifically modularity and global efficiency. These metrics were calculated using the Brain Connectivity Toolbox, a MATLAB-based toolbox for structural and functional MRI network analysis (Rubinov & Sporns, 2010). Inputs to the Brain Connectivity Toolbox were the correlation matrices for each timepoint.

First, modularity was calculated for each time point. Modularity is a measure of the number of intra-network connections as compared to the number of intra-network connections expected in a random graph, and quantifies the strength of segregation into distinct networks. Higher modularity values represent stronger network segregation. Modularity (Q) is defined as follows:

$$Q = \sum_{i=1}^{m} (e_{ii} - a_i^2)$$

Where m is the overall number of modules, e_{ii} is the fraction of edges that connect two nodes within module i with respect to the number of all edges in the graph, and a_i is the fraction of edges that connect a node in module i to any node in the graph.

Second, global efficiency was calculated for each time point. Global efficiency is the average inverse of the shortest path length for each node to all other nodes. Higher global efficiency is indicative of a higher efficiency of information transfer, or greater network integration. Global efficiency is defined as follows:

$$E_{global} = \frac{1}{N(N-1)} \sum_{i \neq j \in G} \frac{1}{L_{i,j}}$$

Where $L_{i,j}$ is the shortest path length between nodes i and j, and N is the number of nodes of graph G.

Similar to previous studies (Fan et al., 2011; Khundrakpam et al., 2013), bootstrap sampling of 1,000 samples for each age group was conducted in order to test for omnibus differences of graph metrics between all age groups via ANOVA. These bootstrap samples were randomly resampled with replacement for the number of subjects in each age group. Each bootstrap sample resulted in a structural covariance matrix used to calculate modularity and global efficiency. Post-hoc Tukey HSD paired t-tests were used to determine significant differences in graph metrics between specific timepoints to correct for multiple comparisons.

Together, these graph theoretical metrics evaluate the extent to which network segregation and integration change from infancy to middle childhood across the 11 time points in this sample. Based on previous studies of structural covariance network organization during infancy (Fan et al., 2011; Nie et al., 2014), simultaneous increases in integration and segregation

were expected between 0-3 years. However, when shifting into childhood at the age of 3 years, network segregation was expected to continue to increase and integration was expected to decrease until 6 years when integration was expected to increase (Khundrakpam et al., 2012; Nie et al., 2013). These hypotheses are in line with previously mentioned empirical evidence, but contrast with the simultaneous increases in segregation and integration from infancy to 5 years modeled by Cao and colleagues (2017).

Subject-based Maturational Coupling

For each subject, the similarity of cortical thickness trajectories across pairs of regions were quantified by a maturational coupling index developed by Khundrakpam and colleagues (2019). The slope of cortical thickness change from one time point to the next time point for one region at a time was compared to the slope of cortical thickness change across the same two time points for another region. The slopes were compared by computing the cosine of the angle between the two slopes. The cosine of the angle for maturational slopes was calculated between time points t_1-t_2, and between time points t_2-t_3. Each time frame's cosine of the angle was multiplied to yield a product called the maturational coupling index for those two regions (see Figure 1c). This resulted in a 64 x 64 maturational coupling matrix for the DK atlas, and a 148 x 148 maturational coupling matrix for the Destrieux atlas for each subject, quantifying the maturational coupling of brain regions for each subject. In order to replicate methods introduced by Khundrakpam and colleagues, only three time points at a time were used for subject-based maturation coupling. Time points across the first year of life (0, 6, and 12 months) were used for one set of analyses of subject-based maturational coupling to assess maturation across the first year when the largest changes occur. Another set of time points across the first two years of life (0, 12, and 24 months) were used for a second set of analyses consistent with time intervals of

previous infant neuroimaging studies. Finally, time points from infancy to middle childhood were used for a third set of analyses (0, 3, and 6 years) to assess more prolonged maturation. These three different sets of sbMCN analyses were used to determine the relevance of early brain development (first year or first two years), as compared to more protracted brain development through childhood (first 6 years), to cognitive outcomes.

Subject-based maturational coupling was calculated for all subjects with collected timepoints at all three timepoints for each age range. As described above, modularity and global efficiency were calculated for each subject-based maturational coupling matrix. The 31 subjects assessed with the DAS-II were median split into two groups based on their DAS-II GCA score so that differences in modularity and global efficiency of subject-based maturational covariance based on reasoning and conceptual abilities could be examined. Modularity and global efficiency were additionally correlated with DAS-II GCA score to determine whether network segregation and integration were related to cognitive outcome at age 5-6. Exploratory analyses related DAS-II subscores (verbal reasoning, non-verbal reasoning, and spatial ability) to whole-brain network measures from sbMCNs, and also related DAS-II subscores to network-specific measures. Specifically, graph metrics of local efficiency and clustering coefficient were used to quantify within-network organization. Local efficiency is a measure of the efficiency of information transfer between node, i, with neighboring nodes in subgraph, G, with a number of nodes, N, and is calculated with the following formula:

$$E_{local}(i) = \frac{1}{N} \sum_{i \in G} E_{global}(G_i)$$

Clustering coefficient at the network level measures the degree to which nodes in a graph cluster, such that k_i is the degree (number of connections) of node *i* and L_i is the number of edges between the k_i neighbors of node *i* calculated with the following formula:

$$C_i = \frac{2Li}{ki(ki-1)}$$

Both local efficiency and clustering coefficient are nodal measures, thus, network local efficiency and clustering coefficient were calculated as the average nodal measures within a given network. The dorsal attention network only had two ROIs and therefore, was unable to be measured with these network metrics. The 6 other networks were used to probe for network-specific relationships.

Another graph metric, participation coefficient (PC), was used to additionally quantify integration given the possible collinearity previously demonstrated in studies of SCNs (Fan et al. 2011; Nie et al., 2013). PC is normalized measure of connections between networks. This is measured by subtracting the ratio of the degree of node i with other nodes in its network, k_{is} to the degree of node i with other nodes regardless of network membership from 1. The formula for PC is as follows:

$$PC_i = 1 - \sum_{s=1}^{N_M} \left(\frac{k_{is}}{k_i}\right)^2$$

Task performance measures at 7-10 years were correlated with modularity and global efficiency from sbMCNs. These task performance measures were response times, response time differences, and inverse efficiency from the SRT, along with accuracy and d' from the n-back task. Additional exploratory analyses were conducted to correlate the same graph metrics of the 6 networks from sbMCNs with task performance. All correlations of cognitive outcomes with

graph metrics measured here were corrected for multiple comparisons using the Benjamini-Hochberg procedure. Specifically, we corrected for three sets of sbMCN analyses with two graph metrics that were correlated with five different measures of task performance, resulting in 30 comparisons overall.

RESULTS

DAS-II

The DAS-II GCA and subscores of verbal reasoning, non-verbal reasoning, and spatial ability were used as cognitive outcomes at 5-6 years for this study (N=31). The DAS-II GCA had a mean of 101.6, standard deviation (SD) of 11.2, range of 77-125, kurtosis of 3.3, and skewness of -0.53. The DAS-II verbal reasoning subscore had a mean of 99.4, SD of 11.3, range of 72-117, kurtosis of 2.5, and skewness of -0.51. The DAS-II non-verbal reasoning subscore had a mean of 98.9, SD of 11.3, range of 73-120, kurtosis of 2.7, and skewness of -0.14. The DAS-II spatial ability subscore had a mean of 105.6, SD of 10.9, range of 85-131, kurtosis of 2.6, and skewness of 0.23.

Task behavior

Task performance on the SRT was measured over both runs using response time (mean = 0.675 seconds, SD = 0.087), response time difference (mean = 0.019, SD = 0.048), and inverse efficiency (mean = 859.6, SD = 268.4). These measures were first analyzed to examine effects of motor learning from the first run of the SRT to the second run. Several participants were excluded based on poor task performance such that they were less than 25% accurate overall on the task (N = 8), which resulted in 24 subjects for subsequent behavioral analysis of the task. A 2 x 2 repeated measures ANOVA was used to test for main effects of run and condition and the

interaction of the two independent variables. There was a significant main effect of run ($F(1,23) = 13.183$, $p = 0.001$) and a significant main effect of condition ($F(1,23) = 6.037$, $p = 0 .022$), but the interaction of run and condition was not significant ($F(1,23) = 0.209$, $p = 0.652$; Figure 7). Post-hoc t-tests revealed that response times for the sequence condition trended towards being faster than the random condition for the first run of the task ($t(23) = -1.654$, $p = 0.111$). For the second run of the task, response times for the sequence condition were significantly faster than the random condition ($t(23) = -2.167$, $p = 0.040$). Only response times of trials that were correctly responded were used for these analyses. However, the response time difference between the random condition and sequence condition from the first run to the second run of the task was not significant ($t(23) = -0.457$, $p = 0.651$). Inverse efficiency was not significantly different between the random and sequence conditions for the first run of the task ($t(23) = -1.215$, $p = 0.236$), nor for the second run of the task ($t(23) = -0.149$, $p = 0.882$), suggesting that a speed-accuracy tradeoff did not occur over the course of the task.

Task performance on the n-back task was assessed using accuracy (0-back: mean = 0.857, SD = 0.121; 2-back: mean = 0.67, SD = 0.200), response time (0-back: mean = 0.701, SD = 0.085; 2-back: mean = 0.770, SD = 0.099), and d' (0-back: mean = 2.713, SD = 0.831; 2-back: mean = 1.332, SD = 0.791). Two subjects who returned for the 7-10 year timepoint were not compliant for the n-back task. Task performance criterion was such that participants must correctly respond to 50% of 0-back trials. However, all participants who completed the n-back task met this criterion (N=30). Overall, the 2-back condition had lower accuracy ($t(29) = 6.06$, $p < 0 .001$), longer response times ($t(29) = -4.612$, $p < 0.001$), and lower d' than the 2-back condition ($t(29) = 8.237$, $p < 0.001$; Figure 8). Lower accuracy and longer response times were found specifically for the 2-back target trials compared to 0-back target trials (i.e. trials with a 2-

back match, or trials with an X for 0-back match; accuracy: ($t(29) = 5.055$, $p < 0.001$); response time: ($t(29) = -3.398$, $p = 0.002$)). These results replicate n-back task effects, such that participants are slower and less accurate for the 2-back condition overall and for target trials (Schleepen & Jonkman, 2009).

Given the potential contributions of age and handedness impacting performance on both of these tasks, linear regression was used to examine the significance of these predictors on task performance. Age was a mean-centered continuous variable and handedness was a categorical variable (0 = Left-handed: N=3, 1 = Right-handed: N=26, N = 3 without handedness information) used to predict each dependent variable of each task. For the SRT task, mean-centered age significantly predicted response time ($B = -0.091$, $p = 0.005$) and inverse efficiency difference ($B = 818.5$, $p = 0.002$), but only trended towards predicting response time difference ($B = 0.050$, $p = 0.069$). Handedness did not predict response time ($B=0.003$, $p = 0.954$), response time difference ($B = -0.015$, $p = 0.751$), or inverse efficiency difference ($B = 652.2$, $p = 0.140$). For the n-back task, neither mean-centered age or handedness predicted 2-back target accuracy (Age: ($B = 0.066$, $p = 0.461$); Handedness: ($B = -0.177$, $p = 0.224$)) or 2-back d' (Age: ($B = -0.319$, $p = 0.379$); Handedness: ($B = -0.169$, $p = 0.771$)). These results suggest that the weak effects of motor learning on this fixed trial pacing version of the SRT task are driven by age-related differences in motor learning, which is consistent with motor learning literature (Hodel et al., 2014; Thomas & Nelson, 2001).

Structural Covariance Networks

At the group level, omnibus group differences were observed for both modularity ($F(10,10,989) = 3690$, $p<0.001$) and global efficiency ($F(10,10989) = 5609$, $p<0.001$) for structural covariance networks using the DK atlas. Omnibus group differences were also

observed for both modularity ($F(10,10,989) = 4710$, $p<0.001$) and global efficiency ($F(10,10989) = 3581$, $p<0.001$) for structural covariance networks using the Destrieux atlas. Increases in modularity (Figure 9) and decreases in global efficiency (Figure 10) were found in the age range of this study. Post-hoc Tukey HSD paired t-tests also revealed that global efficiency significant increased between year five to year six in this sample using both the DK and Destrieux atlases ($p<0.001$, see Table 2 and Table 4). Post-hoc Tukey HSD paired t-tests for modularity are also reported for both atlases in Table 1 and Table 3. Given the possible redundancy of modularity and global efficiency measured with these SCNs, we also then examined the correlation of modularity and global efficiency. We found they were negatively correlated with each other for all timepoints for both atlases ($p<0.001$, see Tables 5 and 6). PC similarly was shown to decrease from 0-6 years with the DK atlas ($F(10,10,989) = 84.62$, $p<0.001$) and with the Destrieux atlas ($F(10,10989) = 122.8$, $p<0.001$; Figure 11). PC was less correlated with modularity than global efficiency was correlated with modularity (see Tables 11 and 12), suggesting a similar pattern of increased segregation and decreased integration. Post-hoc t-tests also revealed PC continued to decrease between 5-6 years, contrary to what was found with global efficiency (see Tables 13 and 14).

Subject-based maturational coupling

At the individual level, there were no group differences in modularity ($t(14.288)= -1.6003$, $p=0.1314$ for 0-1 sbMCN; $t(23.362)= -0.054675$, $p=0.9569$ for 0-2 sbMCN; $t(25.063)= -1.032$, $p=0.3119$ for 0-6 sbMCN) or global efficiency ($t(20.075)= 1.116$, $p=0.2776$ for 0-1 sbMCN; $t(24.998)= -0.79504$, $p=0.434$ for 0-2 sbMCN; $t(27.76)= 0.060135$, $p=0.9525$ for 0-6 sbMCN) when subjects were median split by DAS-II GCA scores at 5-6 years (n=31). Additionally, modularity ($r= 0.2637274$, $p= 0.1838$ for 0-1 sbMCN; $r= -0.0132064$, $p= 0.9479$

for 0-2 sbMCN; r= 0.1499137, p= 0.4291 for 0-6 sbMCN) and global efficiency (r= -0.1179493, p= 0.5579 for 0-1 sbMCN; r= 0.01973306, p= 0.9222 for 0-2 sbMCN; r= 0.01841838, p= 0.923 for 0-6 sbMCN) were not correlated with the GCA score. Exploratory analyses correlating graph metrics of sbMCNs with the GCA subscores did not reveal any significant relationships (See Table 7). Further, exploratory analyses correlating graph metrics of sbMCNs for the 6 networks with the GCA score and subscores did not reveal any significant relationships (See Table 8).

Next, we assessed the relationship between network organization using sbMCNs and task performance at 7-10 years. No significant correlations between network organization of sbMCNs from 0-1 years with task performance were found (n= 27 for SRT; n=26 for n-back). For the time range of 0-2 years, modularity of sbMCNs demonstrated a negative correlation with the response time difference between random and sequence conditions on the second run of the SRT (n=28; r = -0.338, p = 0.078, p-value adjusted = 0.527, see Figure 12). This correlation did not remain significant when correcting for multiple comparisons. Global efficiency of sbMCNs from 0-2 years was not correlated with performance on either the SRT (n=28) or n-back (n=27) tasks.

For the time range of 0-6 years, global efficiency of sbMCNs was positively correlated with 2-back target accuracy (n=26, r = 0.770, p < 0.001, p-value adjusted for FDR < 0.001, see Figure 13), as well as trended positively with d' of the 2-back condition (r = 0.533, p = 0.005, p-value adjusted = 0.075, see Figure 14). In this same time range, modularity of sbMCNs also trended negatively with 2-back target accuracy (r = -0.495, p = 0.010, p-value adjusted = 0.010, see Figure 15). Modularity or global efficiency of sbMCNs from 0-6 years were not correlated with performance on the SRT task (See Table 9). Exploratory analyses that correlated graph metrics (local efficiency and clustering coefficient) of sbMCNs for six Yeo networks with task performance revealed that no specific networks were related with task performance during any

timeframe (0-1, 0-2, 0-2; all p's > 0.05; see Table 9). The effect of age and handedness was included in regression models with additional predictors of modularity and global efficiency from 0-6 sbMCNs predicting n-back performance, which still revealed global efficiency was the only significant predictor of working memory performance (*Regression of 2-back target accuracy*: Age: B = 0.026, p = 0.675; Handedness: B = -0.025, p = 0.796; Modularity: B = 5.495, p = 0.151; Global Efficiency: B = 52.104, p < 0.001. *Regression of 2-back d'*: Age: B = -0.324, p = 0.340; Handedness: B = 0.340, p = 0.519; Modularity: B = 16.28, p = 0.407; Global Efficiency: B = 143.63, p = 0.034).

DISCUSSION

Here, for the first time, we observed brain network organizational changes from infancy to childhood within the same sample of subjects and related those changes to individual level predictions of cognition. As expected, modularity of structural covariance networks increased beyond year two. Global efficiency of structural covariance networks decreased after year two. Examining network organization of subject-based maturational coupling during early development revealed that modularity did not relate to motor learning performance on the SRT task at 7-10 years when correcting for multiple comparisons. Additionally, global efficiency of subject-based maturational coupling from infancy to six years was strongly correlated with working memory accuracy on the n-back task at 7-10 years. However, subject-based maturational coupling of specific networks was not related to performance on either SRT or n-back tasks, nor the DAS-II. These results are in line with previous studies that broadly demonstrate positive relationships between network integration with cognition (Cohen & D'Esposito, 2016; Finc et al., 2017), and help extend these relationships to a developmental

period when children undergo increasing specialization and integration of cognitive processes (Johnson & Munakata, 2005).

The group level changes of network organization reported here help explain how cortical thickness matures from infancy to childhood. Given that the cortical thickness of most cortical regions were positively correlated across subjects for structural covariance networks at birth in this sample, this global similarity is likely the reason for higher levels of global efficiency initially at birth. This suggests that cortical morphology initially is not differentiated into distinct, coherent networks. However, with the pronounced increases in modularity seen at age two, cortical networks are thought to become differentiated as regions in the same network share similar levels of cortical thickness across subjects. Global efficiency was shown to decrease at this time from two years to five years. The mechanism of synaptic pruning, which likely drives these network changes, is known to increase at the age of two and is thought to eliminate redundant or unnecessary connections nearby and distant (Huttenlocher et al., 1982; Petanjek et al., 2011). Long-range connections between distant and distinct networks should survive synaptic pruning and instead become strengthened via myelination to allow for more efficient information transfer between networks (Baum et al., 2017). These processes take time (i.e. on the scale of years) and is likely why we see network integration increasing at six years and beyond in this study and other studies.

The lack of a relationship between organization of sbMCNs for all time frames (0-1, 0-2, and 0-6) and DAS II GCA scores was contrary to our hypotheses that both modularity and global efficiency would positively be related to general cognition at 5-6 years. This null finding highlights that patterns of network organization may specifically relate to certain cognitive processes (e.g. motor learning and working memory), not general cognitive outcome measures

like the DAS II GCA score. The DAS II has been mostly used to assess typical and atypical development (Elliot, 2007), and may not provide the specificity as the tasks used here.

The earlier segregation of structural covariance found at the group level suggested that individual variation in segregation at this time would be related to a cognitive process that relies on a single network like motor learning, however, we did not find this relationship to be significant. A lack of a structural correspondence to motor learning found here is not necessarily inconsistent with existing literature of functional network correspondence to motor learning and execution. Bassett and colleagues have demonstrated that greater modular organization of functional brain networks facilitated the learning of a motor sequence practiced over several sessions (2015). Individual level variation of modularity derived from function brain networks during a motor execution task has also revealed modularity was positively related to response time variability (Cohen & D'Esposito, 2016). Modularity in the present study was measured from the maturational coupling of cortical thickness networks and was not measured from functional networks during the task like the two aforementioned studies. The timescales of neural change are different between structural and functional modalities. For this reason, maturational change observed over the scale of years may not demonstrate a relationship to later motor learning in this study as it does with brain function during a motor task observed at the scale of minutes in other studies. Future work is needed to examine changes in segregation of brain structure and function to better understand how these different timescales contribute to motor learning.

On the other hand, the time-specific relations of global efficiency of sbMCNs from infancy to six years also reveal how protracted maturational coupling supports later working memory. The working memory required to perform the n-back task, especially in higher working

memory loads like the 2-back condition assessed here, is likely the result of several cognitive processes like encoding, maintaining, and manipulating information spread across several distinct brain networks (e.g. visual, somatomotor, frontoparietal). We reported a lack of a significant correlation of global efficiency from sbMCNs during 0-1 years and 0-2 years with n-back performance at 7-10 years, yet, strong positive correlations for global efficiency of sbMCNs during 0-6 years with 2-back target accuracy at 7-10 years. This set of results provides evidence that increasing network integration over the first six years of life is critical for later working memory at 7-10 years. Previous work has also generally shown that integrated brain networks during childhood support working memory and other executive functions requiring the integration of information (Baum et al., 2017; Marek et al., 2015).

The limitations and inconsistences of the present study should be considered with respect to the study's sample characteristics and imaging modality. Previous developmental network neuroscience studies have yet to link early brain development to middle childhood within a single sample, which limits the understanding of how and when developmental changes in network organization occur. The coverage between infancy and to childhood is a rare strength of this dataset. However, the relatively small sample size and participant dropout for later timepoints reduces the statistical power and should be considered with respect to the claims made from this study. The ongoing data collection with this sample will also help verify if network integration continues to increase at 7-10 years old. Additionally, imaging modalities of brain function and structure appear to have slight differences when it comes to measuring graph theory metrics like modularity and global efficiency. Whether it be due to neural properties or methodological consequence of fMRI, functional activity of one region is known to be spatially autocorrelated with another nearby region. As a result, functional connectivity has been shown to

have a stronger relationship with closer anatomical distance than structural and maturational covariance, which led to higher clustering and modularity for functional networks than their respective structural and maturational covariance networks (Alexander-Bloch et al., 2013). Relatedly, motion impacts the ability to accurately detect structural and functional connectivity across development, and influences the ability to accurately measure cortical thickness (Baum et al., 2018; Grayson & Fair, 2017; Satterthwaite et al., 2013). It still remains unclear how motion may influence structural covariance and maturational coupling in this and other studies. This warrants further research examining multimodal trajectories of brain network organization to determine if the pattern of network organizational changes during early development shown here is consistent or different for brain structure and function.

This study has furthered understanding of the cognitive relevance of early brain network development in several ways. Cortical thickness network organizational changes appear to map onto cognitive processes of specialization and integration during infancy and childhood as supported by theoretical claims made by Johnson and Munakata (2005) and empirical work on cortical thickness networks across the age ranges of infancy to childhood (Fan et al., 2011; Nie et al., 2013). Initially, infants may process information in a global manner that is computationally redundant. But with time, brain networks become specialized for certain cognitive computations. One network provides a special computation that another network is not as well-suited for. Different networks become more distinct, yet, complementary. These networks can then increasingly come together to support complex executive functions like working memory. Network organizational changes can be observed at the group and individual levels using measures of cortical thickness as shown here, and correspond to later cognitive performance. Most importantly, this study demonstrates that a child's current cognitive functioning is reliant

on how that child's brain development has occurred over time. Future work should continue to examine the cognitive relevance of brain network development, not only to predict later cognition but also to map network organization during infancy and childhood onto concurrent cognitive functioning.

TABLES

Table 1. Tukey HSD post-hoc t-tests of modularity for SCNs using the DK atlas

Timepoint contrast	Adjusted p-value
3-0	<0.001
6-0	<0.001
9-0	0.115
12-0	<0.001
18-0	0.002
24-0	<0.001
36-0	<0.001
48-0	<0.001
60-0	<0.001
72-0	<0.001
6-3	<0.001
9-3	<0.001
12-3	<0.001
18-3	<0.001
24-3	<0.001
36-3	<0.001
48-3	<0.001
60-3	<0.001
72-3	<0.001
9-6	<0.001
12-6	<0.001
18-6	0.009
24-6	<0.001
36-6	<0.001
48-6	<0.001
60-6	<0.001
72-6	<0.001
12-9	0.011
18-9	<0.001
24-9	<0.001
36-9	<0.001
48-9	<0.001
60-9	<0.001
72-9	<0.001
18-12	<0.001
24-12	<0.001
36-12	<0.001
48-12	<0.001
60-12	<0.001
72-12	<0.001

24-18	<0.001
36-18	<0.001
48-18	<0.001
60-18	<0.001
72-18	<0.001
36-24	<0.001
48-24	0.999
60-24	<0.001
72-24	<0.001
48-36	<0.001
60-36	<0.001
72-36	<0.001
60-48	<0.001
72-48	<0.001
72-60	<0.001

Table 2. Tukey HSD post-hoc t-tests of global efficiency for SCNs using the DK atlas

Timepoint contrast	Adjusted p-value
3-0	<0.001
6-0	<0.001
9-0	<0.001
12-0	<0.001
18-0	<0.001
24-0	<0.001
36-0	<0.001
48-0	<0.001
60-0	<0.001
72-0	<0.001
6-3	<0.001
9-3	<0.001
12-3	<0.001
18-3	<0.001
24-3	<0.001
36-3	<0.001
48-3	<0.001
60-3	<0.001
72-3	<0.001
9-6	<0.001
12-6	<0.001
18-6	0.999
24-6	<0.001
36-6	<0.001
48-6	<0.001
60-6	<0.001
72-6	<0.001
12-9	0.531
18-9	<0.001
24-9	<0.001
36-9	<0.001
48-9	<0.001
60-9	<0.001
72-9	<0.001
18-12	<0.001
24-12	<0.001
36-12	<0.001
48-12	<0.001
60-12	<0.001
72-12	<0.001
24-18	<0.001
36-18	<0.001

48-18	<0.001
60-18	<0.001
72-18	<0.001
36-24	<0.001
48-24	<0.001
60-24	<0.001
72-24	<0.001
48-36	<0.001
60-36	<0.001
72-36	0.566
60-48	<0.001
72-48	<0.001
72-60	<0.001

Table 3. Post-hoc t-tests of modularity for SCNs using the Destrieux atlas

Timepoint contrast	Adjusted p-value
3-0	<0.001
6-0	<0.001
9-0	0.378
12-0	0.458
18-0	<0.001
24-0	<0.001
36-0	<0.001
48-0	<0.001
60-0	<0.001
72-0	<0.001
6-3	<0.001
9-3	<0.001
12-3	<0.001
18-3	0.024
24-3	<0.001
36-3	<0.001
48-3	<0.001
60-3	<0.001
72-3	<0.001
9-6	<0.001
12-6	<0.001
18-6	<0.001
24-6	<0.001
36-6	<0.001
48-6	<0.001
60-6	<0.001
72-6	<0.001
12-9	<0.001
18-9	<0.001
24-9	<0.001
36-9	<0.001
48-9	<0.001
60-9	<0.001
72-9	<0.001
18-12	<0.001
24-12	<0.001
36-12	<0.001
48-12	<0.001
60-12	<0.001
72-12	<0.001
24-18	<0.001
36-18	<0.001

48-18	<0.001
60-18	<0.001
72-18	<0.001
36-24	<0.001
48-24	0.304
60-24	<0.001
72-24	<0.001
48-36	<0.001
60-36	<0.001
72-36	<0.001
60-48	<0.001
72-48	<0.001
72-60	<0.001

Table 4. Tukey post-hoc t-tests of global efficiency for SCNs using the Destrieux atlas

Timepoint contrast	Adjusted p-value
3-0	<0.001
6-0	<0.001
9-0	0.003
12-0	<0.001
18-0	<0.001
24-0	<0.001
36-0	<0.001
48-0	<0.001
60-0	<0.001
72-0	<0.001
6-3	<0.001
9-3	<0.001
12-3	<0.001
18-3	0.001
24-3	<0.001
36-3	<0.001
48-3	<0.001
60-3	<0.001
72-3	<0.001
9-6	<0.001
12-6	<0.001
18-6	<0.001
24-6	<0.001
36-6	<0.001
48-6	<0.001
60-6	<0.001
72-6	<0.001
12-9	0.999
18-9	<0.001
24-9	<0.001
36-9	<0.001
48-9	<0.001
60-9	<0.001
72-9	<0.001
18-12	<0.001
24-12	<0.001
36-12	<0.001
48-12	<0.001
60-12	<0.001
72-12	<0.001
24-18	<0.001
36-18	<0.001

48-18	<0.001
60-18	<0.001
72-18	<0.001
36-24	<0.001
48-24	<0.001
60-24	<0.001
72-24	<0.001
48-36	<0.001
60-36	<0.001
72-36	<0.001
60-48	<0.001
72-48	<0.001
72-60	<0.001

Table 5. Correlations of modularity and global efficiency for each timepoint using the DK atlas.

Age	r-value	p-value
0	-0.826	<0.001
3	-0.784	<0.001
6	-0.656	<0.001
9	-0.806	<0.001
12	-0.767	<0.001
18	-0.726	<0.001
24	-0.840	<0.001
36	-0.512	<0.001
48	-0.760	<0.001
60	-0.679	<0.001
72	-0.748	<0.001

Table 6. Correlations of modularity and global efficiency for each timepoint using the Destrieux atlas.

Age	r-value	p-value
0	-0.788	<0.001
3	-0.709	<0.001
6	-0.624	<0.001
9	-0.806	<0.001
12	-0.765	<0.001
18	-0.770	<0.001
24	-0.809	<0.001
36	-0.105	<0.001
48	-0.632	<0.001
60	-0.546	<0.001
72	-0.591	<0.001

Table 7. Correlations of sbMCNs with DAS subscores.

Correlation	r-value	p-value
sbMCN 0-1		
Modularity & Verbal Reasoning	0.2637274	0.1838
Modularity & Nonverbal Reasoning	0.2018569	0.3126
Modularity & Spatial Ability	0.3076256	0.1185
GE & Verbal Reasoning	-0.1179493	0.5579
GE & Nonverbal Reasoning	-0.2891621	0.1435
GE & Spatial Ability	-0.2928175	0.1383
sbMCN 0-2		
Modularity & Verbal Reasoning	-0.0132064	0.9479
Modularity & Nonverbal Reasoning	0.1741045	0.3851
Modularity & Spatial Ability	-0.0392138	0.846
GE & Verbal Reasoning	0.01973306	0.9222
GE & Nonverbal Reasoning	-0.1765524	0.3784
GE & Spatial Ability	-0.04225504	0.8342
sbMCN 0-6		
Modularity & Verbal Reasoning	0.1499137	0.4291
Modularity & Nonverbal Reasoning	-0.1458562	0.4419
Modularity & Spatial Ability	-0.194188	0.3038
GE & Verbal Reasoning	0.01841838	0.923
GE & Nonverbal Reasoning	-0.07180389	0.7061
GE & Spatial Ability	0.04824523	0.8001

Table 8. Correlations of graph metrics for 6 sbMCNs with DAS subscores.

Local efficiency			Clustering Coefficient		
Correlation	r-value	p-value adj	Correlation	r-value	p-value adj.
0-1 sbMCN & Verbal Reasoning					
Visual	0.03134903	p > 0.05	Visual	0.02619136	p > 0.05
Somatomotor	0.0968375	p > 0.05	Somatomotor	0.07205197	p > 0.05
Ventral Attention	0.09375196	p > 0.05	Ventral Attention	0.08816563	p > 0.05
Limbic	0.1876178	p > 0.05	Limbic	0.2094845	p > 0.05
Frontoparietal	0.1876178	p > 0.05	Frontoparietal	-0.3059213	p > 0.05
Default	-0.2518823	p > 0.05	Default	-0.2608088	p > 0.05
0-1 sbMCN & Nonverbal Reasoning					
Visual	-0.04966948	p > 0.05	Visual	-0.05338354	p > 0.05
Somatomotor	0.03698405	p > 0.05	Somatomotor	0.01027283	p > 0.05
Ventral Attention	0.002825075	p > 0.05	Ventral Attention	0.01646792	p > 0.05
Limbic	0.3491368	p > 0.05	Limbic	0.3569417	p > 0.05
Frontoparietal	-0.3267486	p > 0.05	Frontoparietal	-0.3333533	p > 0.05
Default	-0.2862324	p > 0.05	Default	-0.2875944	p > 0.05
0-1 sbMCN & Spatial Ability					
Visual	-0.256586	p > 0.05	Visual	-0.2498471	p > 0.05
Somatomotor	0.1574488	p > 0.05	Somatomotor	0.1549713	p > 0.05
Ventral Attention	-0.1800895	p > 0.05	Ventral Attention	-0.1752671	p > 0.05
Limbic	0.03421389	p > 0.05	Limbic	0.04089014	p > 0.05
Frontoparietal	-0.05892823	p > 0.05	Frontoparietal	-0.03123782	p > 0.05
Default	-0.2135118	p > 0.05	Default	-0.1594562	p > 0.05
0-2 sbMCN & Verbal Reasoning					
Visual	-0.284034	p > 0.05	Visual	-0.291566	p > 0.05
Somatomotor	0.2925012	p > 0.05	Somatomotor	0.2942413	p > 0.05
Ventral Attention	0.07226115	p > 0.05	Ventral Attention	0.06507522	p > 0.05
Limbic	-0.2176608	p > 0.05	Limbic	-0.2300447	p > 0.05
Frontoparietal	0.06344555	p > 0.05	Frontoparietal	0.06451554	p > 0.05
Default	-0.1057886	p > 0.05	Default	-0.1177116	p > 0.05
0-2 sbMCN & Nonverbal Reasoning					
Visual	-0.4241674	p > 0.05	Visual	-0.427467	p > 0.05
Somatomotor	0.1283908	p > 0.05	Somatomotor	0.1365598	p > 0.05
Ventral Attention	-0.02561234	p > 0.05	Ventral Attention	-0.02625234	p > 0.05
Limbic	0.03640272	p > 0.05	Limbic	0.01802603	p > 0.05
Frontoparietal	0.04094406	p > 0.05	Frontoparietal	0.06430286	p > 0.05
Default	-0.1243733	p > 0.05	Default	-0.1167361	p > 0.05

0-2 sbMCN & Spatial Ability					
Visual	-0.3086113	p > 0.05	Visual	-0.3136332	p > 0.05
Somatomotor	0.04838952	p > 0.05	Somatomotor	0.07725028	p > 0.05
Ventral Attention	-0.1690537	p > 0.05	Ventral Attention	-0.1782044	p > 0.05
Limbic	-0.1542045	p > 0.05	Limbic	-0.1354613	p > 0.05
Frontoparietal	0.1262159	p > 0.05	Frontoparietal	0.1422918	p > 0.05
Default	0.002765272	p > 0.05	Default	-0.0014108	p > 0.05
0-6 sbMCN & Verbal Reasoning					
Visual	0.0599785	p > 0.05	Visual	0.06213686	p > 0.05
Somatomotor	0.03285252	p > 0.05	Somatomotor	0.04238902	p > 0.05
Ventral Attention	-0.209235	p > 0.05	Ventral Attention	-0.2116533	p > 0.05
Limbic	-0.2151151	p > 0.05	Limbic	-0.2400892	p > 0.05
Frontoparietal	-0.1850186	p > 0.05	Frontoparietal	-0.1635924	p > 0.05
Default	-0.08955453	p > 0.05	Default	-0.1007756	p > 0.05
0-6 sbMCN & Nonverbal Reasoning					
Visual	0.1244753	p > 0.05	Visual	0.1225344	p > 0.05
Somatomotor	0.1353407	p > 0.05	Somatomotor	0.1426322	p > 0.05
Ventral Attention	-0.1444558	p > 0.05	Ventral Attention	-0.1589319	p > 0.05
Limbic	-0.1002896	p > 0.05	Limbic	-0.1282838	p > 0.05
Frontoparietal	-0.2616193	p > 0.05	Frontoparietal	-0.2698794	p > 0.05
Default	-0.03480925	p > 0.05	Default	-0.0512105	p > 0.05
0-6 sbMCN & Spatial Ability					
Visual	-0.06755134	p > 0.05	Visual	-0.07803936	p > 0.05
Somatomotor	0.1098909	p > 0.05	Somatomotor	0.1136651	p > 0.05
Ventral Attention	-0.4299652	p > 0.05	Ventral Attention	-0.4366658	p > 0.05
Limbic	-0.1282919	p > 0.05	Limbic	-0.1662982	p > 0.05
Frontoparietal	0.1646696	p > 0.05	Frontoparietal	0.1726968	p > 0.05
Default	0.1365412	p > 0.05	Default	0.1087934	p > 0.05

Table 9. Correlation of sbMCNs with task performance

Correlation	r-value	p-value adj.
sbMCN 0-1		
Modularity & SRT RTs	0.1219218	p > 0.05
Modularity & SRT RT difference	-0.1872472	p > 0.05
Modularity & SRT Inverse Efficiency difference	0.1555499	p > 0.05
Modularity & 2-back target accuracy	0.2160208	p > 0.05
Modularity & 2-back d’	0.3293901	p > 0.05
GE & SRT RTs	-0.05987114	p > 0.05
GE & SRT RT difference	0.2517518	p > 0.05
GE & SRT Inverse efficiency difference	-0.00566014	p > 0.05
GE& 2-back target accuracy	0.0559946	p > 0.05
GE & 2-back d’	-0.1128163	p > 0.05
sbMCN 0-2		
Modularity & SRT RTs	0.2372867	p > 0.05
Modularity & SRT RT difference	-0.3385358	p > 0.05
Modularity & SRT Inverse Efficiency difference	0.1202638	p > 0.05
Modularity & 2-back target accuracy	0.02769419	p > 0.05
Modularity & 2-back d’	0.1722473	p > 0.05
GE & SRT RTs	0.1723787	p > 0.05
GE & SRT RT difference	0.1748838	p > 0.05
GE & SRT Inverse efficiency difference	0.1127381	p > 0.05
GE& 2-back target accuracy	-0.2081265	p > 0.05
GE & 2-back d’	-0.09296301	p > 0.05
sbMCN 0-6		
Modularity & SRT RTs	0.09333666	p > 0.05
Modularity & SRT RT difference	0.1492336	p > 0.05
Modularity & SRT Inverse Efficiency difference	-0.02235425	p > 0.05
Modularity & 2-back target accuracy	-0.4955081	0.100521
Modularity & 2-back d’	-0.2909311	p > 0.05
GE & SRT RTs	-0.1689373	p > 0.05
GE & SRT RT difference	-0.1088281	p > 0.05
GE & SRT Inverse efficiency difference	0.06110787	p > 0.05
GE& 2-back target accuracy	0.7707408	0.000122
GE & 2-back d’	0.5332386	0.075456

Table 10. Correlation of subnetwork sbMCNs with task performance

Local efficiency			Clustering Coefficient		
Correlation	r-value	p-value adj	Correlation	r-value	p-value adj.
0-1 sbMCN & SRT RT					
Visual	-0.09268262	p > 0.05	Visual	-0.06159578	p > 0.05
Somatomotor	0.1121019	p > 0.05	Somatomotor	0.1171121	p > 0.05
Ventral Attention	-0.2135465	p > 0.05	Ventral Attention	-0.2010719	p > 0.05
Limbic	0.1299773	p > 0.05	Limbic	0.1973339	p > 0.05
Frontoparietal	0.167167	p > 0.05	Frontoparietal	0.1636776	p > 0.05
Default	-0.0074548	p > 0.05	Default	0.02352395	p > 0.05
0-1 sbMCN & SRT RT difference					
Visual	0.3258516	p > 0.05	Visual	0.3146997	p > 0.05
Somatomotor	0.1557805	p > 0.05	Somatomotor	0.1537761	p > 0.05
Ventral Attention	0.00879262	p > 0.05	Ventral Attention	-0.0081107	p > 0.05
Limbic	-0.07364193	p > 0.05	Limbic	-0.126593	p > 0.05
Frontoparietal	0.04810831	p > 0.05	Frontoparietal	0.05125806	p > 0.05
Default	0.08512552	p > 0.05	Default	0.06759464	p > 0.05
0-1 sbMCN & SRT Inv. Eff. difference					
Visual	0.1762208	p > 0.05	Visual	0.1752194	p > 0.05
Somatomotor	-0.05339298	p > 0.05	Somatomotor	-0.04035533	p > 0.05
Ventral Attention	-0.1568074	p > 0.05	Ventral Attention	-0.1366699	p > 0.05
Limbic	0.1759249	p > 0.05	Limbic	0.1529378	p > 0.05
Frontoparietal	-0.1188831	p > 0.05	Frontoparietal	-0.1163481	p > 0.05
Default	0.1842576	p > 0.05	Default	0.1976917	p > 0.05
0-1 sbMCN & 2-back target accuracy					
Visual	-0.1806602	p > 0.05	Visual	-0.1903088	p > 0.05
Somatomotor	0.07466963	p > 0.05	Somatomotor	0.07414269	p > 0.05
Ventral Attention	-0.2929205	p > 0.05	Ventral Attention	-0.2960357	p > 0.05
Limbic	0.1052484	p > 0.05	Limbic	0.05269093	p > 0.05
Frontoparietal	-0.01873856	p > 0.05	Frontoparietal	0.00277059	p > 0.05
Default	-0.01905071	p > 0.05	Default	-0.0276799	p > 0.05
0-1 sbMCN & 2-back d’					
Visual	-0.2914465	p > 0.05	Visual	-0.2919591	p > 0.05
Somatomotor	0.08016935	p > 0.05	Somatomotor	0.09004955	p > 0.05
Ventral Attention	-0.529987	p > 0.05	Ventral Attention	-0.5245122	p > 0.05
Limbic	-0.1474021	p > 0.05	Limbic	-0.1318593	p > 0.05
Frontoparietal	0.2706297	p > 0.05	Frontoparietal	0.2979928	p > 0.05
Default	0.1273796	p > 0.05	Default	0.1457753	p > 0.05

0-2 sbMCN & SRT RT					
Visual	0.1560412	p > 0.05	Visual	0.05349349	p > 0.05
Somatomotor	0.1121559	p > 0.05	Somatomotor	0.08254162	p > 0.05
Ventral Attention	-0.2801963	p > 0.05	Ventral Attention	-0.2630382	p > 0.05
Limbic	0.2754445	p > 0.05	Limbic	0.2527246	p > 0.05
Frontoparietal	-0.1051161	p > 0.05	Frontoparietal	-0.09981498	p > 0.05
Default	-0.1019717	p > 0.05	Default	-0.1087377	p > 0.05
0-2 sbMCN & SRT RT difference					
Visual	0.1910852	p > 0.05	Visual	0.1494091	p > 0.05
Somatomotor	0.2886223	p > 0.05	Somatomotor	0.2591143	p > 0.05
Ventral Attention	-0.1196258	p > 0.05	Ventral Attention	-0.1323826	p > 0.05
Limbic	-0.07495317	p > 0.05	Limbic	-0.05310436	p > 0.05
Frontoparietal	0.09142673	p > 0.05	Frontoparietal	0.07390396	p > 0.05
Default	0.2831347	p > 0.05	Default	0.2779317	p > 0.05
0-2 sbMCN & SRT Inv. Eff. difference					
Visual	-0.1811013	p > 0.05	Visual	-0.2161813	p > 0.05
Somatomotor	0.3213175	p > 0.05	Somatomotor	0.3190773	p > 0.05
Ventral Attention	0.06974911	p > 0.05	Ventral Attention	0.05997035	p > 0.05
Limbic	-0.06624381	p > 0.05	Limbic	-0.06293867	p > 0.05
Frontoparietal	-0.2552992	p > 0.05	Frontoparietal	-0.2518014	p > 0.05
Default	0.09100853	p > 0.05	Default	0.09186326	p > 0.05
0-2 sbMCN & 2-back target accuracy					
Visual	-0.09293319	p > 0.05	Visual	-0.01636055	p > 0.05
Somatomotor	-0.2586455	p > 0.05	Somatomotor	-0.2515219	p > 0.05
Ventral Attention	-0.0228344	p > 0.05	Ventral Attention	-0.01669747	p > 0.05
Limbic	-0.05246215	p > 0.05	Limbic	-0.05992748	p > 0.05
Frontoparietal	-0.1159426	p > 0.05	Frontoparietal	-0.1051937	p > 0.05
Default	0.07449614	p > 0.05	Default	0.08682715	p > 0.05
0-2 sbMCN & 2-back d’					
Visual	-0.1776157	p > 0.05	Visual	-0.187946	p > 0.05
Somatomotor	-0.1341125	p > 0.05	Somatomotor	-0.1400557	p > 0.05
Ventral Attention	-0.2118277	p > 0.05	Ventral Attention	-0.2024424	p > 0.05
Limbic	0.05500019	p > 0.05	Limbic	0.05194442	p > 0.05
Frontoparietal	-0.2897975	p > 0.05	Frontoparietal	-0.2715463	p > 0.05
Default	0.04329435	p > 0.05	Default	0.04922735	p > 0.05
0-6 sbMCN & SRT RT					
Visual	0.203626	p > 0.05	Visual	0.2055781	p > 0.05
Somatomotor	-0.08797168	p > 0.05	Somatomotor	-0.07714533	p > 0.05
Ventral Attention	0.04106504	p > 0.05	Ventral Attention	0.05942916	p > 0.05
Limbic	0.4620266	p > 0.05	Limbic	0.4729836	p > 0.05

Frontoparietal	-0.333108	p > 0.05	Frontoparietal	-0.3429996	p > 0.05
Default	-0.00279866	p > 0.05	Default	0.00206661	p > 0.05
0-6 sbMCN & SRT RT difference					
Visual	-0.3016024	p > 0.05	Visual	-0.3036721	p > 0.05
Somatomotor	0.3078282	p > 0.05	Somatomotor	0.3071661	p > 0.05
Ventral Attention	0.08728066	p > 0.05	Ventral Attention	0.08672617	p > 0.05
Limbic	-0.2139696	p > 0.05	Limbic	-0.21281	p > 0.05
Frontoparietal	0.4832403	p > 0.05	Frontoparietal	0.5017257	p > 0.05
Default	0.1311747	p > 0.05	Default	0.1294066	p > 0.05
0-6 sbMCN & SRT Inv. Eff. difference					
Visual	-0.2552272	p > 0.05	Visual	-0.2513871	p > 0.05
Somatomotor	0.4827253	p > 0.05	Somatomotor	0.4904747	p > 0.05
Ventral Attention	0.3500845	p > 0.05	Ventral Attention	0.3339656	p > 0.05
Limbic	0.01967116	p > 0.05	Limbic	-0.0081923	p > 0.05
Frontoparietal	0.00166723	p > 0.05	Frontoparietal	0.00231158	p > 0.05
Default	0.0106466	p > 0.05	Default	0.01596516	p > 0.05
0-6 sbMCN & 2-back target accuracy					
Visual	0.2806085	p > 0.05	Visual	0.2467341	p > 0.05
Somatomotor	0.2318846	p > 0.05	Somatomotor	0.2107754	p > 0.05
Ventral Attention	-0.3406925	p > 0.05	Ventral Attention	-0.363434	p > 0.05
Limbic	-0.4233591	p > 0.05	Limbic	-0.4523898	p > 0.05
Frontoparietal	0.03512662	p > 0.05	Frontoparietal	0.02292206	p > 0.05
Default	-0.2092523	p > 0.05	Default	-0.2769934	p > 0.05
0-6 sbMCN & 2-back d’					
Visual	0.3088514	p > 0.05	Visual	0.2863733	p > 0.05
Somatomotor	0.0774431	p > 0.05	Somatomotor	0.06022321	p > 0.05
Ventral Attention	-0.4560004	p > 0.05	Ventral Attention	-0.4680479	p > 0.05
Limbic	-0.1951835	p > 0.05	Limbic	-0.216246	p > 0.05
Frontoparietal	-0.03970668	p > 0.05	Frontoparietal	-0.05776902	p > 0.05
Default	-0.1813635	p > 0.05	Default	-0.2203371	p > 0.05

Table 11. Correlation of modularity and participation coefficient for DK atlas

Age	r-value	p-value
0	-0.0602	<0.001
3	-0.172	<0.001
6	-0.151	<0.001
9	-0.0702	<0.001
12	-0.158	<0.001
18	-0.289	<0.001
24	-0.366	<0.001
36	-0.427	<0.001
48	-0.299	<0.001
60	-0.484	<0.001
72	-0.458	<0.001

Table 12. Correlation of modularity and participation coefficient with Destrieux atlas

Age	r-value	p-value
0	-0.315	<0.001
3	-0.301	<0.001
6	-0.217	<0.001
9	-0.123	<0.001
12	-0.164	<0.001
18	-0.299	<0.001
24	-0.432	<0.001
36	-0.488	<0.001
48	-0.422	<0.001
60	-0.340	<0.001
72	-0.509	<0.001

Table 13. Tukey HSD post-hoc t-tests for participation coefficient with the DK atlas

3-0	<0.001
6-0	<0.001
9-0	<0.001
12-0	<0.001
18-0	<0.001
24-0	<0.001
36-0	<0.001
48-0	0.49475805
60-0	<0.001
72-0	<0.001
6-3	<0.001
9-3	0.00138885
12-3	<0.001
18-3	<0.001
24-3	0.05426163
36-3	<0.001
48-3	0.16163925
60-3	<0.001
72-3	<0.001
9-6	0.00134988
12-6	<0.001
18-6	<0.001
24-6	<0.001
36-6	0.07195607
48-6	<0.001
60-6	0.99981066
72-6	0.04140071
12-9	<0.001
18-9	<0.001
24-9	0.9957736
36-9	0.99080182
48-9	<0.001
60-9	0.02008596
72-9	<0.001
18-12	0.80779267
24-12	<0.001
36-12	<0.001
48-12	<0.001
60-12	<0.001
72-12	0.02199762
24-18	<0.001
36-18	<0.001
48-18	<0.001

60-18	<0.001
72-18	0.82477754
36-24	0.57347915
48-24	<0.001
60-24	<0.001
72-24	<0.001
48-36	<0.001
60-36	0.36849906
72-36	<0.001
60-48	<0.001
72-48	<0.001
72-60	0.00336741

Table 14. Tukey HSD post-hoc t-tests for participation coefficient with the Destrieux atlas

3-0	0.57893789
6-0	< 0.001
9-0	< 0.001
12-0	< 0.001
18-0	0.99993019
24-0	< 0.001
36-0	< 0.001
48-0	< 0.001
60-0	< 0.001
72-0	< 0.001
6-3	< 0.001
9-3	0.09295948
12-3	< 0.001
18-3	0.92957737
24-3	< 0.001
36-3	< 0.001
48-3	< 0.001
60-3	< 0.001
72-3	< 0.001
9-6	< 0.001
12-6	< 0.001
18-6	< 0.001
24-6	0.99999992
36-6	< 0.001
48-6	< 0.001
60-6	0.58576966
72-6	< 0.001
12-9	< 0.001
18-9	< 0.001
24-9	< 0.001
36-9	< 0.001
48-9	0.51139098
60-9	< 0.001
72-9	< 0.001
18-12	< 0.001
24-12	< 0.001
36-12	< 0.001
48-12	< 0.001
60-12	< 0.001
72-12	0.99990017
24-18	< 0.001
36-18	< 0.001
48-18	< 0.001

60-18	< 0.001
72-18	< 0.001
36-24	< 0.001
48-24	< 0.001
60-24	0.3680107
72-24	< 0.001
48-36	< 0.001
60-36	< 0.001
72-36	< 0.001
60-48	< 0.001
72-48	< 0.001
72-60	< 0.001

Figure 1. A flowchart demonstrating how cortical thickness network edges can be measured both across and within subjects. Panel 1a illustrates the construction of a structural covariance network (SCN), which measures edges between nodes as the correlation of cortical thickness across subjects. Panel 1b illustrates the construction of a maturational covariance network (MCN), which measures edges between nodes as the correlation of maturational slopes across subjects. Panel 1c illustrates the construction of subject-based maturational coupling (sbMC), which measures edges between nodes as the maturational coupling index (MCI) for subsequent network analysis of sbMCNs. Panel 1c is adapted from Khundrakpam et al., 2019.

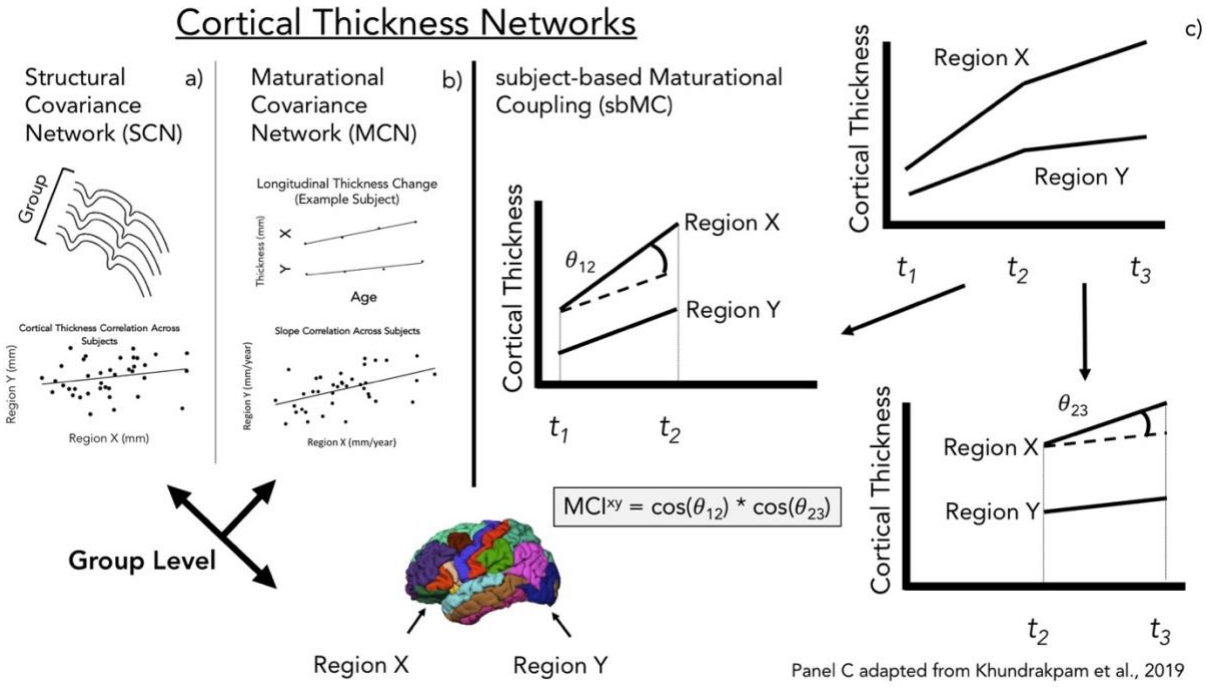

Figure 2. A longitudinal plot demonstrating the distribution of timepoints per subject labeled by sex. Additional information of the number of subjects, average, SD, and range in days for each timepoint is also presented.

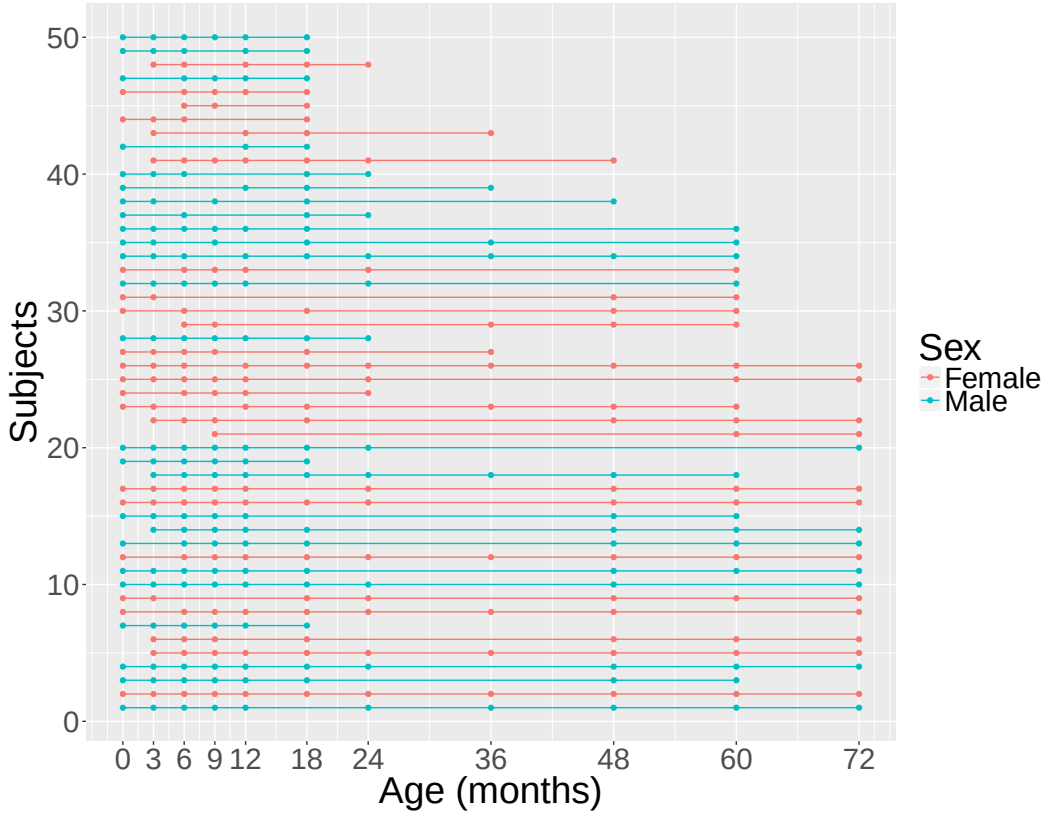

Age	0	3	6	9	12	18	24	36	48	60	72
N=	39	36	41	36	36	40	23	14	26	28	19
Average (days)	27.3	94.6	190	277.9	375.7	556.8	738	1101.1	1472.7	1861.6	2211.1
SD (days)	9.0	8.6	12.8	13.6	14.6	19.8	27.3	18.2	18.2	42.2	26.1
Range (days)	34	35	56	58	66	106	131	69	75	193	105

Figure 3. An illustration of the paradigm used for the Serial Reaction Time Task (SRT). Participants were told to indicate the location of an ‘X’ presented on the screen by a button press.

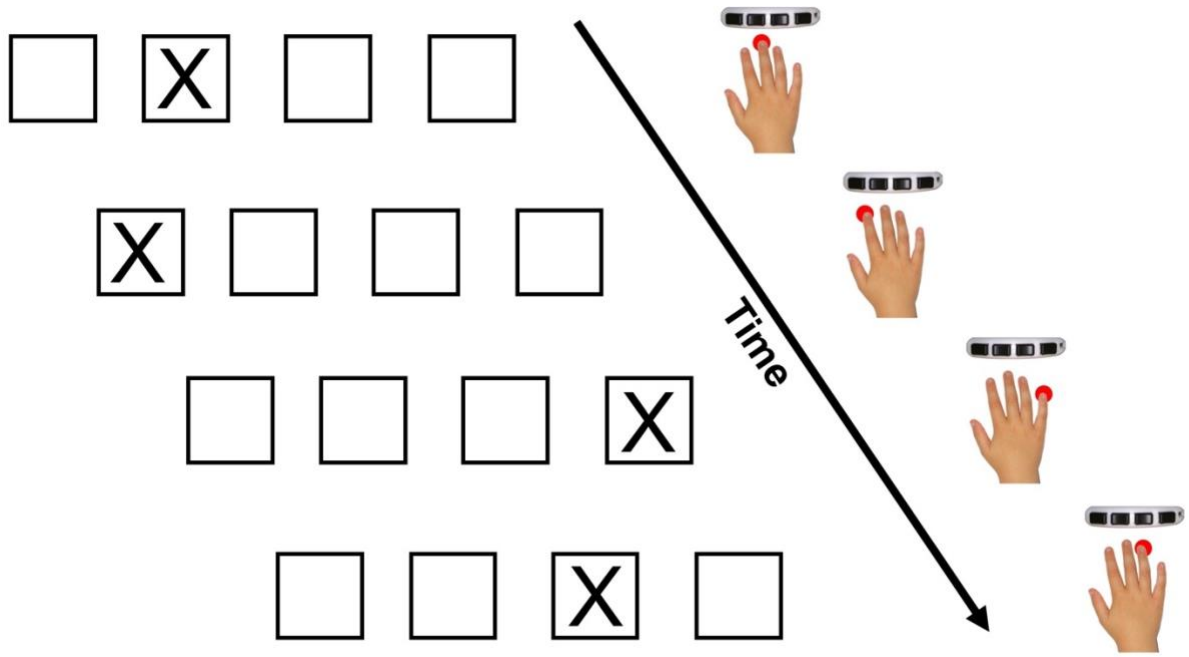

Figure 4. An illustration of the paradigm used for the n-back task with 0-back and 2-back conditions. Participants were told to respond with a button press whether the current stimulus was the same as (a ‘match’) or different from (a ‘non-match’) the stimulus seen n previously. For the 0-back condition, ‘X’ was used as a ‘match’ and any other letter was a ‘non-match’. For the 2-back condition, participants responded whether the current stimulus was a ‘match’ or a ‘non-match’ to the letter presented two previously.

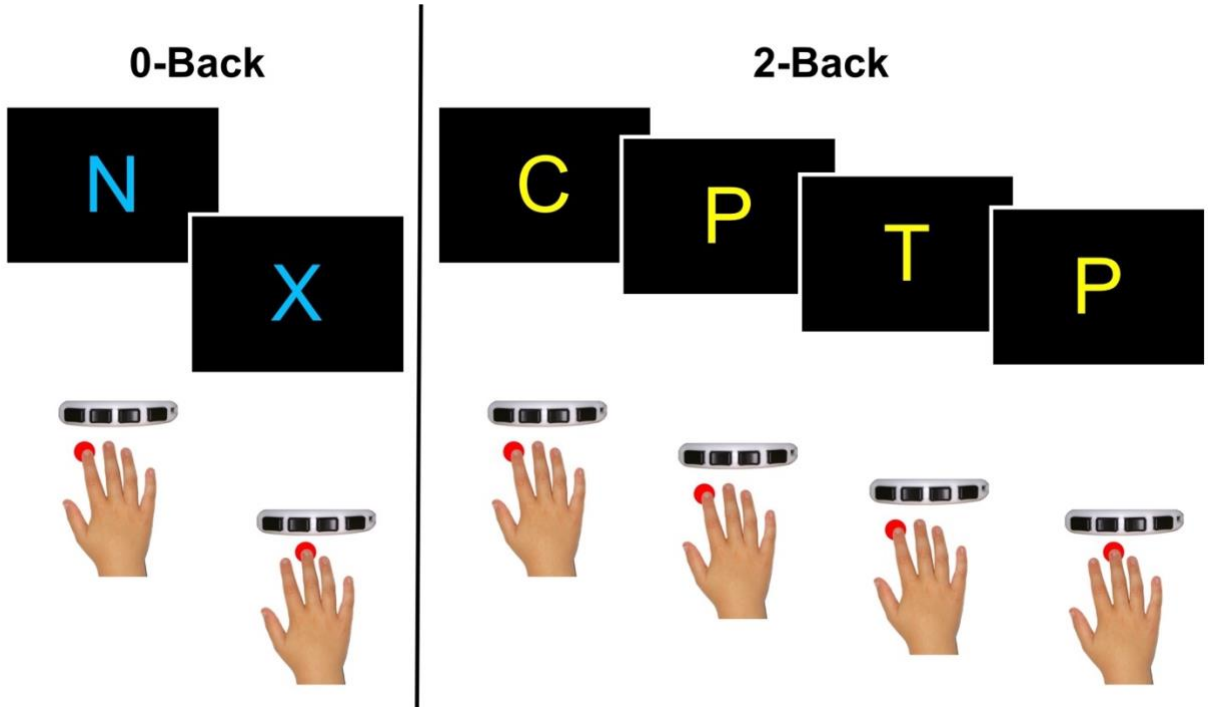

Figure 5. A visual flowchart of the imaging pipeline used for this longitudinal dataset. Figure adapted from Li et al. (2018).

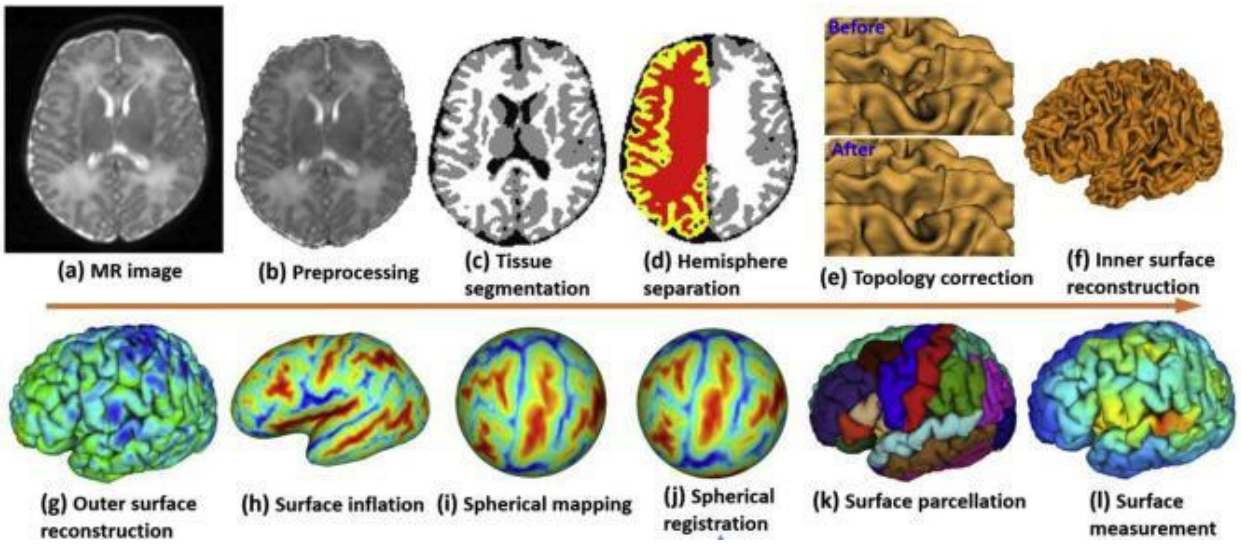

Figure 6. An illustration of the 7 previously defined brain networks taken from Yeo et al., 2011.

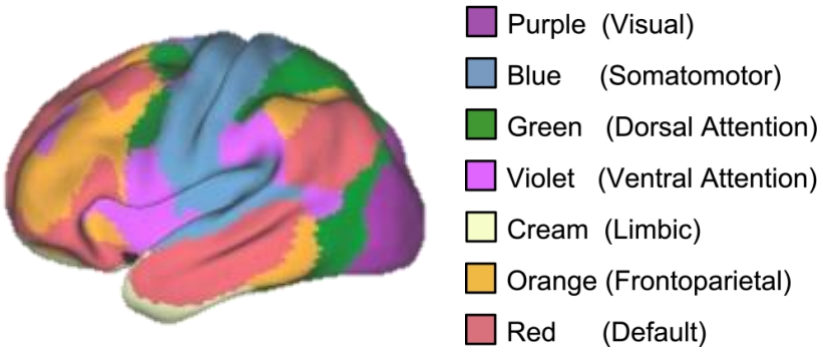

Figure 7. Response times from run to run by condition for the SRT task. Significant main effects of run and condition were observed, however, the interaction of run and condition was not significant. Error bars represent standard error.

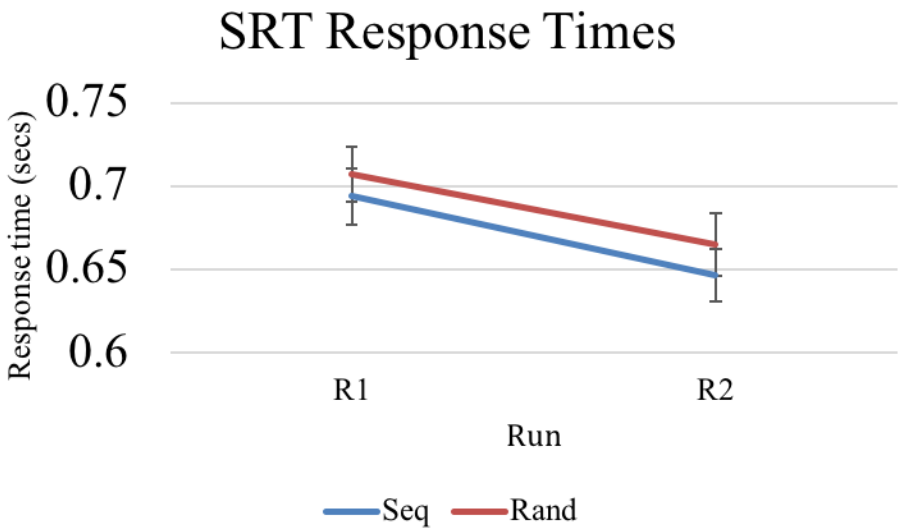

Figure 8. Behavioral results for the n-back task. Overall accuracy and response times of the 0-back and 2-back conditions of the n-back task are illustrated in the top panel. The middle panel demonstrates accuracy and response times of 0-back and 2-back target trials. The bottom panel demonstrates d' for 0-back and 2-back conditions. Error bars represent standard error.

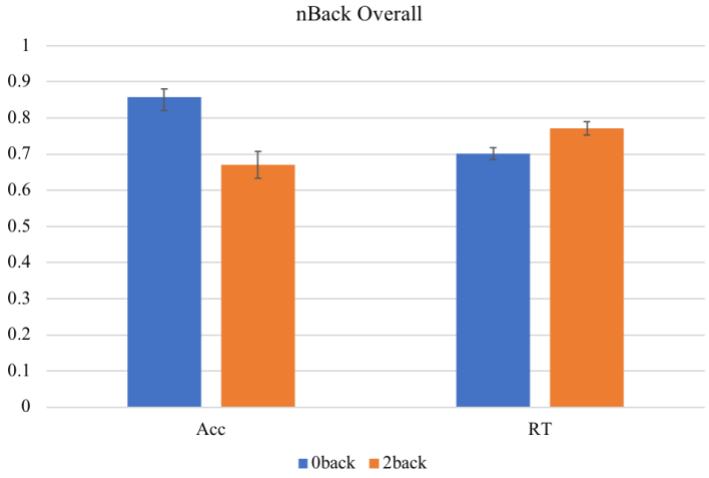

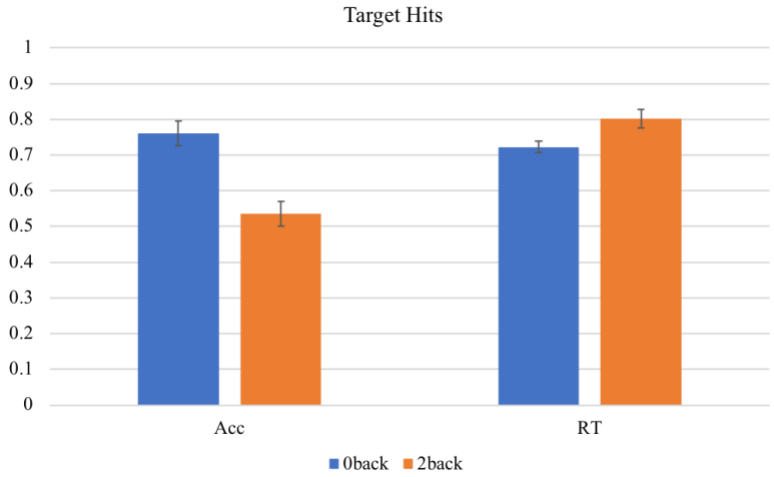

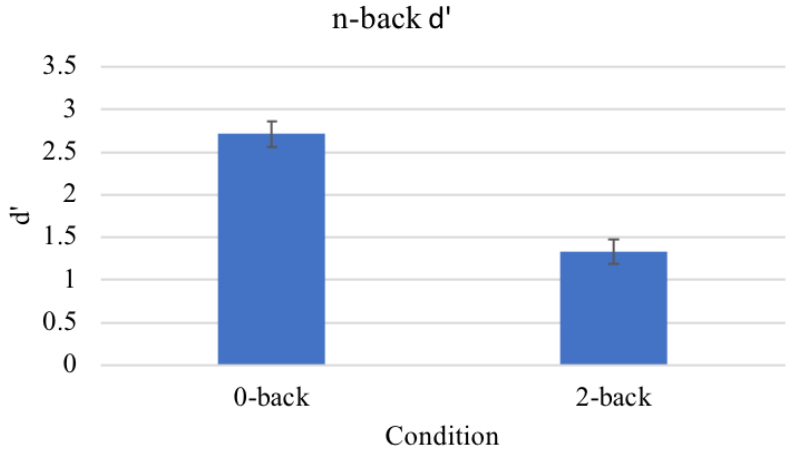

Figure 9. Modularity of SCNs increased from birth to six years. Top figure represents modularity measured from the DK atlas, and bottom figure represents modularity measured from the Destrieux atlas. Box plots represent the mean and quartiles of observed distributions. Outliers are represented with dots.

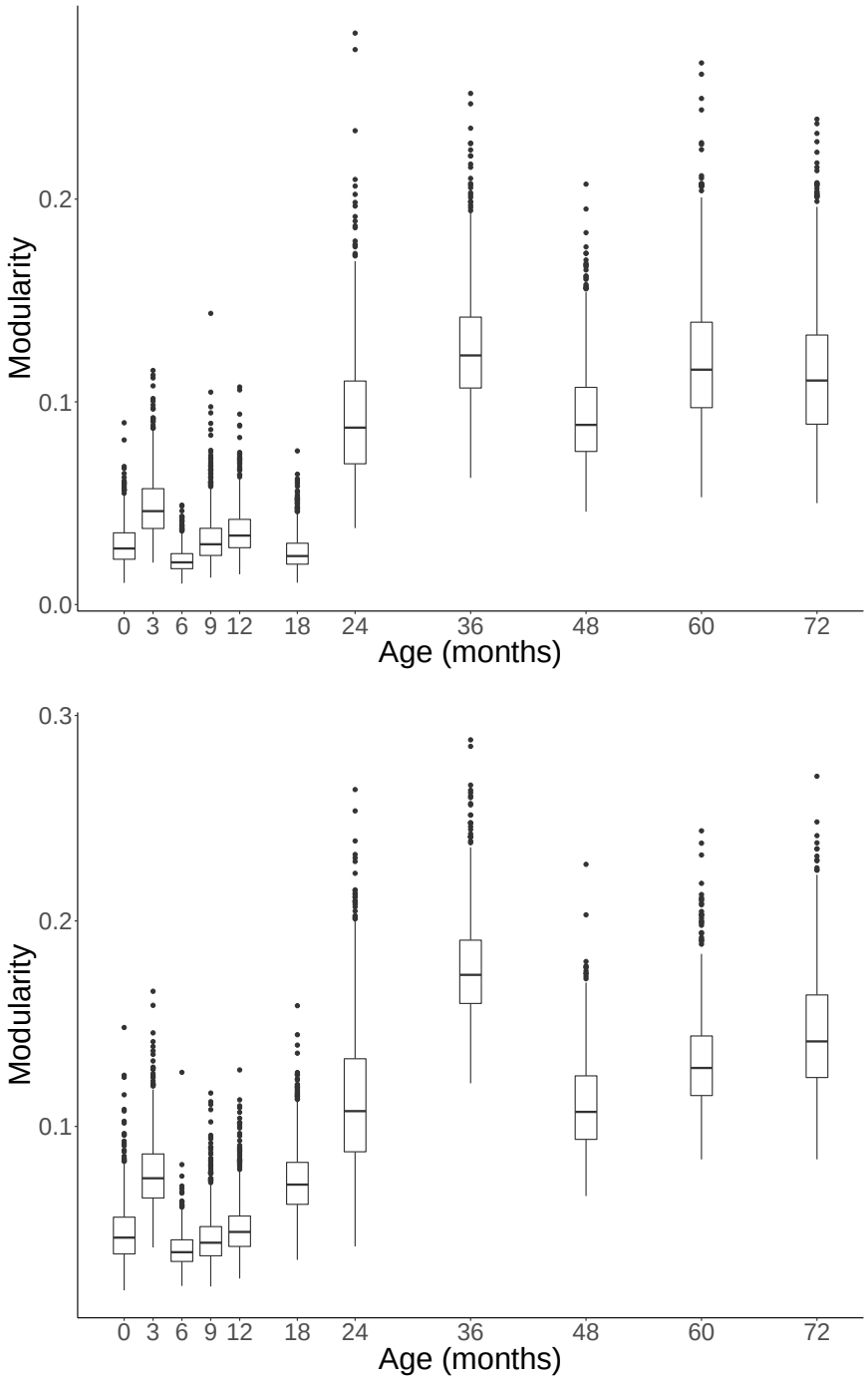

Figure 10. Global efficiency of SCNs from the Destrieux atlas decreased from birth to five years, and increased at six years. Top figure represents global efficiency measured from the DK atlas, and bottom figure represents global efficiency measured from the Destrieux atlas. Box plots represent the mean and quartiles of observed distributions. Outliers are represented with dots.

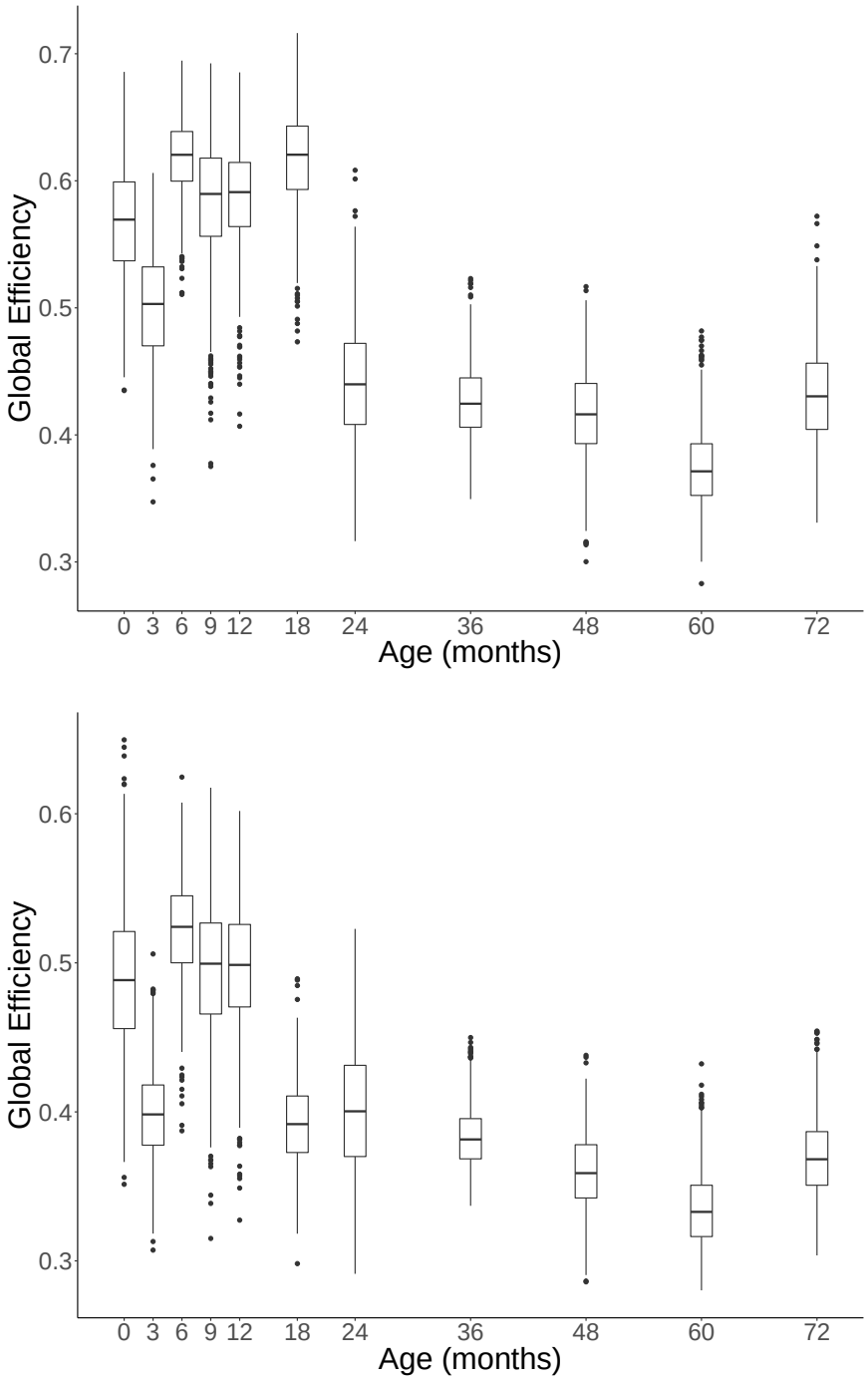

Figure 11. PC of SCNs decreased from birth to six years. Top figure represents PC measured from the DK atlas, and bottom figure represents PC measured from the Destrieux atlas. Box plots represent the mean and quartiles of observed distributions. Outliers are represented with dots.

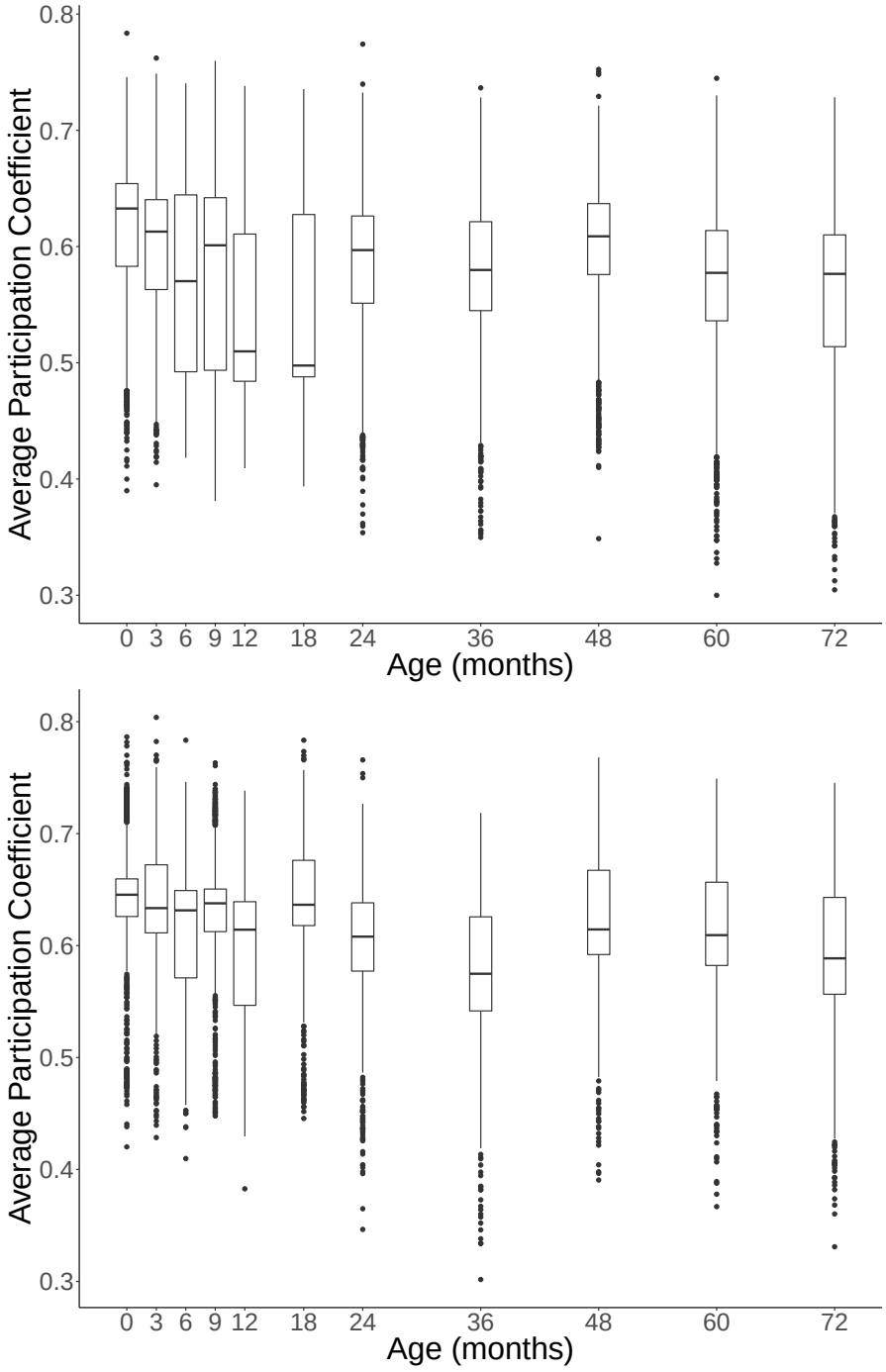

Figure 12. Subject-based maturational coupling during infancy did not significantly relate to motor learning performance. This scatterplot demonstrates modularity of sbMCNs from 0-2 years was negatively correlated with the SRT RT difference between random and sequence conditions on the second run of the SRT, but this relationship did not remain significant when correcting for multiple comparisons.

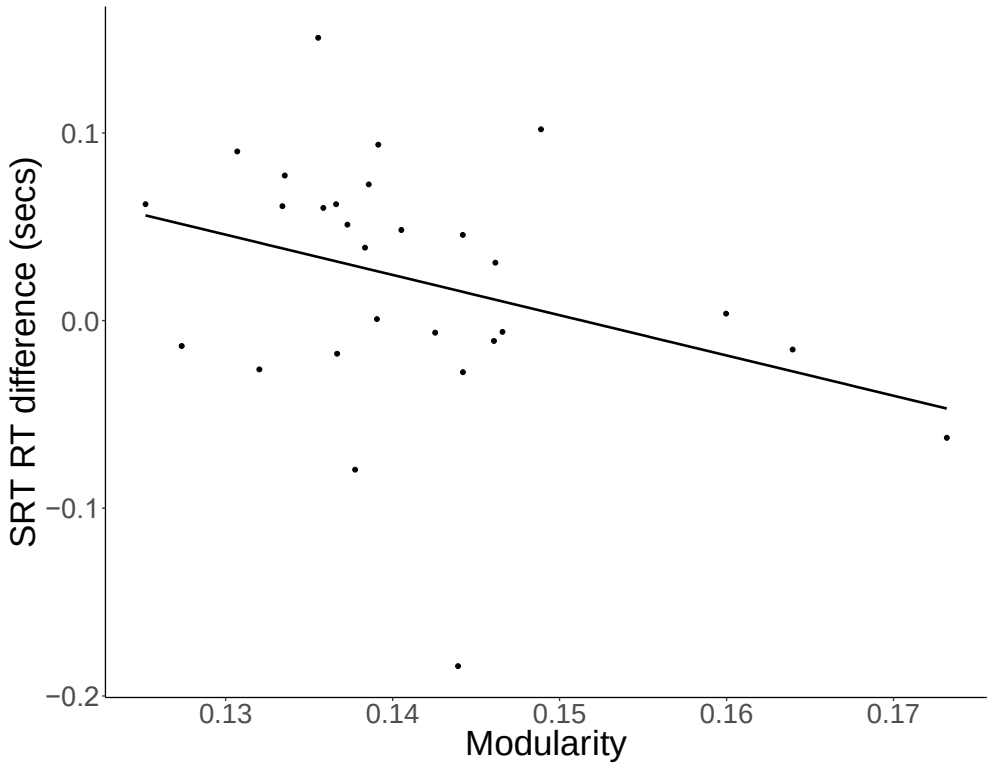

Figure 13. Global efficiency of sbMCNs from 0-6 years was positively correlated with 2-back target accuracy.

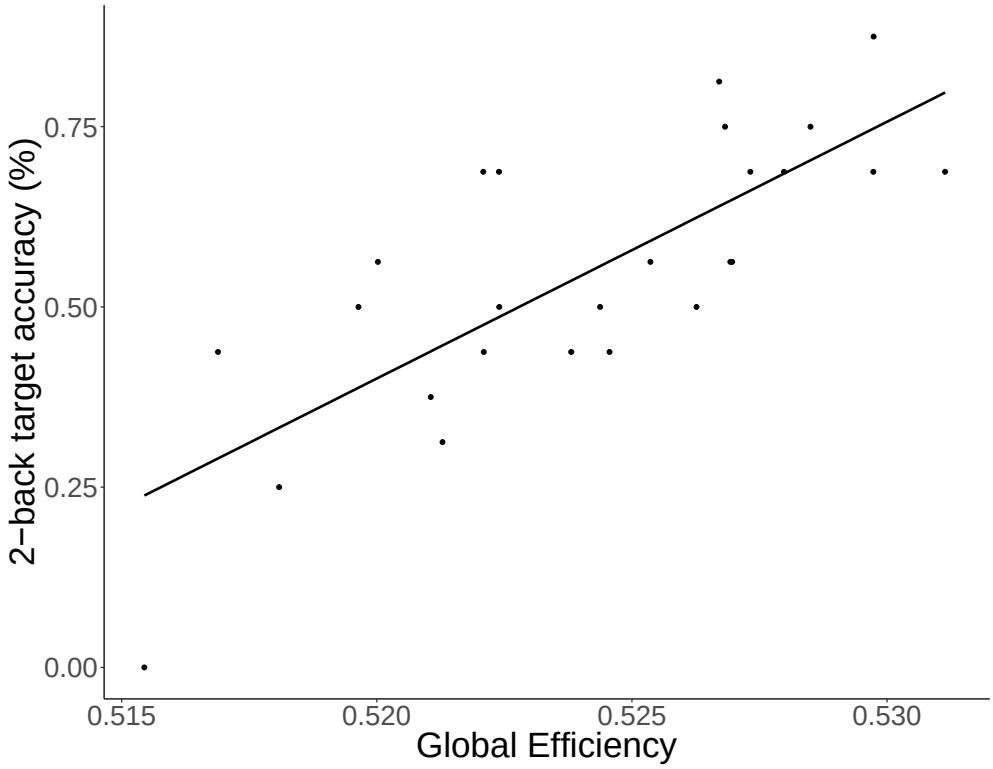

Figure 14. Global efficiency of sbMCNs from 0-6 years trended positively with d' of the 2-back condition.

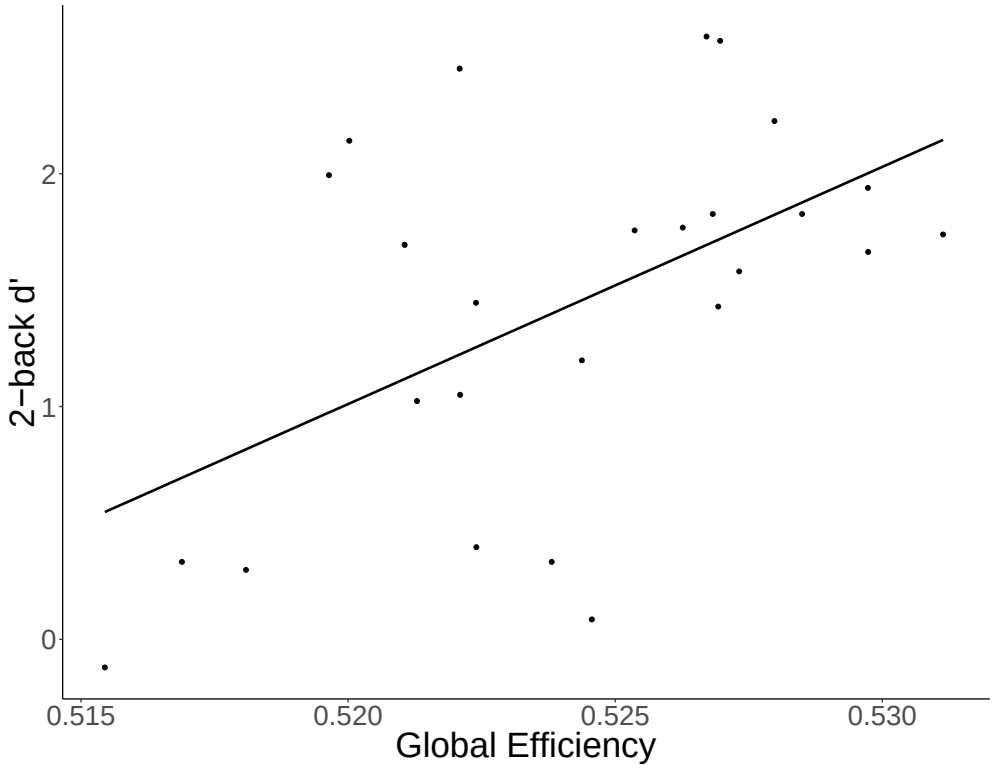

Figure 15. Modularity of sbMCNs from 0-6 years trended negatively with 2-back target accuracy.

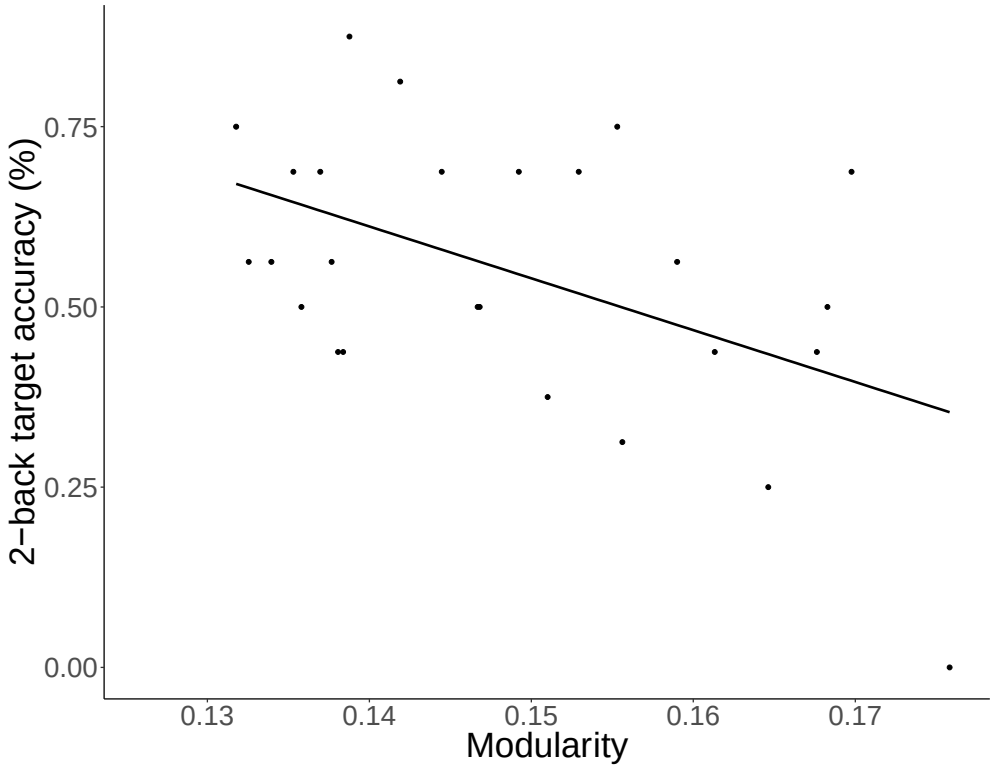

REFERENCES

Alexander-Bloch, A., Giedd, J. N., & Bullmore, E. (2013). Imaging structural co-variance between human brain regions. *Nature Reviews Neuroscience*, *14*(5), 322-336.

Alexander-Bloch, A., Raznahan, A., Bullmore, E., & Giedd, J. (2013). The convergence of maturational change and structural covariance in human cortical networks. *Journal of Neuroscience*, *33*(7), 2889-2899.

Baddeley, A. (1992). Working memory. *Science*, *255*(5044), 556-559.

Bassett, D. S., Wymbs, N. F., Rombach, M. P., Porter, M. A., Mucha, P. J., & Grafton, S. T. (2013). Task-based core-periphery organization of human brain dynamics. *PLoS computational biology*, *9*(9), e1003171.

Bassett, D. S., Yang, M., Wymbs, N. F., & Grafton, S. T. (2015). Learning-induced autonomy of sensorimotor systems. *Nature neuroscience*, *18*(5), 744.

Baum, G. L., Ciric, R., Roalf, D. R., Betzel, R. F., Moore, T. M., Shinohara, R. T., Kahn, A.E., Vandekar, S.N., Rupert, P.E., Quarmley, M., & Cook, P. A. (2017). Modular Segregation of Structural Brain Networks Supports the Development of Executive Function in Youth. *Current Biology*.

Baum, G. L., Roalf, D. R., Cook, P. A., Ciric, R., Rosen, A. F., Xia, C., Elliott, M.A., Ruparel, K., Verma, R., Tunç, B., & Gur, R. C. (2018). The impact of in-scanner head motion on structural connectivity derived from diffusion MRI. *Neuroimage*, *173*, 275-286.

Best, J. R., & Miller, P. H. (2010). A developmental perspective on executive function. *Child development*, *81*(6), 1641-1660.

Bethlehem, R. A., Romero-Garcia, R., Mak, E., Bullmore, E. T., & Baron-Cohen, S. (2017). Structural covariance networks in children with autism or ADHD. *Cerebral Cortex*, *27*(8), 4267-4276.

Cao, M., Huang, H., & He, Y. (2017). Developmental connectomics from infancy through early childhood. *Trends in Neurosciences*, 40(8), 494-506.

Chen, Z. J., He, Y., Rosa-Neto, P., Gong, G., & Evans, A. C. (2011). Age-related alterations in the modular organization of structural cortical network by using cortical thickness from MRI. *NeuroImage*, *56*(1), 235-245.

Ciesielski, K. T., Lesnik, P. G., Savoy, R. L., Grant, E. P., & Ahlfors, S. P. (2006). Developmental neural networks in children performing a Categorical N-Back Task. *Neuroimage*, *33*(3), 980-990.

Cohen, J. R. (2018). The behavioral and cognitive relevance of time-varying, dynamic changes in functional connectivity. *NeuroImage*, *180*, 515-525.

Cohen, J. R., & D'Esposito, M. (2016). The segregation and integration of distinct brain networks and their relationship to cognition. *Journal of Neuroscience*, 36(48), 12083-12094.

Cohen, J. R., & Poldrack, R. A. (2008). Automaticity in motor sequence learning does not impair response inhibition. *Psychonomic bulletin & review*, *15*(1), 108-115.

D'Souza, H., Cowie, D., Karmiloff-Smith, A., & Bremner, A. J. (2017). Specialization of the motor system in infancy: from broad tuning to selectively specialized purposeful actions. *Developmental Science*, *20*(4), e12409.

Dean, D. C., Dirks, H., O'Muircheartaigh, J., Walker, L., Jerskey, B. A., Lehman, K., Han, M., Waskiewicz, N., & Deoni, S. C. (2014). Pediatric neuroimaging using magnetic resonance imaging during non-sedated sleep. *Pediatric radiology*, *44*(1), 64-72.

Desikan, R. S., Ségonne, F., Fischl, B., Quinn, B. T., Dickerson, B. C., Blacker, D., Buckner, R.L., Dale, A.M., Maguire, R.P., Hyman, B.T., & Albert, M. S. (2006). An automated labeling system for subdividing the human cerebral cortex on MRI scans into gyral based regions of interest. *Neuroimage*, *31*(3), 968-980.

Destrieux, C., Fischl, B., Dale, A., & Halgren, E. (2010). Automatic parcellation of human cortical gyri and sulci using standard anatomical nomenclature. *Neuroimage*, *53*(1), 1-15.

Elliott, C. D. (2007). *Differential Ability Scales* (2nd ed.). San Antonio, TX: Harcourt Assessment.

Fair, D. A., Cohen, A. L., Power, J. D., Dosenbach, N. U., Church, J. A., Miezin, F. M., Schlaggar, B.L. & Petersen, S. E. (2009). Functional brain networks develop from a "local to distributed" organization. *PLoS computational biology*, *5*(5), e1000381.

Fan, Y., Shi, F., Smith, J. K., Lin, W., Gilmore, J. H., & Shen, D. (2011). Brain anatomical networks in early human brain development. *NeuroImage*, *54*(3), 1862–1871.

Finc, K., Bonna, K., Lewandowska, M., Wolak, T., Nikadon, J., Dreszer, J., Duch, W. & Kühn, S. (2017). Transition of the functional brain network related to increasing cognitive demands. *Human brain mapping*, *38*(7), 3659-3674.

Fischl, B. (2012). FreeSurfer. *Neuroimage*, *62*(2), 774-781.

Gao, W., Gilmore, J. H., Giovanello, K. S., Smith, J. K., Shen, D., Zhu, H., & Lin, W. (2011). Temporal and spatial evolution of brain network topology during the first two years of life. *PloS one*, *6*(9), e25278.

Gao, W., Alcauter, S., Elton, A., Hernandez-Castillo, C. R., Smith, J. K., Ramirez, J., & Lin, W. (2014). Functional network development during the first year: relative sequence and socioeconomic correlations. *Cerebral Cortex*, 25(9), 2919-2928.

Gao, W., Alcauter, S., Smith, J. K., Gilmore, J. H., & Lin, W. (2015). Development of human brain cortical network architecture during infancy. *Brain Structure and Function*, 220(2), 1173- 1186.

Gao, W., Lin, W., Grewen, K., & Gilmore, J. H. (2017). Functional connectivity of the infant human brain: Plastic and modifiable. *Neuroscientist*, *23*(2), 169–184.

Gilmore, J. H., Knickmeyer, R. C., & Gao, W. (2018). Imaging structural and functional brain development in early childhood. *Nature Reviews Neuroscience*, *19*(3), 123.

Grayson, D. S., & Fair, D. A. (2017). Development of large-scale functional networks from birth to adulthood: A guide to the neuroimaging literature. *NeuroImage*.

Hodel, A. S., Markant, J. C., Van Den Heuvel, S. E., Cirilli-Raether, J. M., & Thomas, K. M. (2014). Developmental differences in effects of task pacing on implicit sequence learning. *Frontiers in psychology*, *5*, 153.

Huttenlocher, P. R. (1990). Morphometric study of human cerebral cortex development. *Neuropsychologia*, 28(6), 517-527.

Huttenlocher, P. R., de Courten, C., Garey, L. J., & Van der Loos, H. (1982). Synaptogenesis in human visual cortex—evidence for synapse elimination during normal development. *Neuroscience letters*, *33*(3), 247-252.

Johnson, M. H. (2000). Functional brain development in infants: Elements of an interactive specialization framework. *Child development*, *71*(1), 75-81.

Johnson, M. H. (2001). Functional brain development in humans. *Nature Reviews Neuroscience*, *2*(7), 475.

Johnson, M. H. (2011). Interactive specialization: a domain-general framework for human functional brain development?. *Developmental cognitive neuroscience*, *1*(1), 7-21.

Johnson, M. H., & Munakata, Y. (2005). Processes of change in brain and cognitive development. Trends in cognitive sciences, 9(3), 152-158.

Johnson, S. P. (2011). Development of visual perception. *Wiley Interdisciplinary Reviews: Cognitive Science*, *2*(5), 515-528.

Khundrakpam, B. S., Lewis, J. D., Jeon, S., Kostopoulos, P., Itturia Medina, Y., Chouinard-Decorte, F., & Evans, A. C. (2019). Exploring Individual Brain Variability during

Development based on Patterns of Maturational Coupling of Cortical Thickness: A Longitudinal MRI Study. *Cerebral Cortex*.

Khundrakpam, B. S., Lewis, J. D., Reid, A., Karama, S., Zhao, L., Chouinard-Decorte, F., Evans, A.C. & Brain Development Cooperative Group. (2017). Imaging structural covariance in the development of intelligence. *Neuroimage*, *144*, 227-240.

Khundrakpam, B. S., Reid, A., Brauer, J., Carbonell, F., Lewis, J., Ameis, S., Karama, S., Lee, J., Chen, Z., Das, S., & Evans, A. C. (2012). Developmental changes in organization of structural brain networks. *Cerebral Cortex*, *23*(9), 2072-2085.

Li, G., Nie, J., Wang, L., Shi, F., Gilmore, J. H., Lin, W., & Shen, D. (2014). Measuring the dynamic longitudinal cortex development in infants by reconstruction of temporally consistent cortical surfaces. *NeuroImage*, *90*, 266-279.

Li, G., Wang, L., Shi, F., Lin, W., & Shen, D. (2014). Simultaneous and consistent labeling of longitudinal dynamic developing cortical surfaces in infants. *Medical image analysis*, *18*(8), 1274-1289.

Li, G., Wang, L., Yap, P. T., Wang, F., Wu, Z., Meng, Y., Dong, P., Kim, J., Shi, F., Rekik, I. & Lin, W. (2018). Computational neuroanatomy of baby brains: A review. *NeuroImage*.

Lin, C. H. J., Knowlton, B. J., Wu, A. D., Iacoboni, M., Yang, H. C., Ye, Y. L., Liu, K.H., & Chiang, M. C. (2016). Benefit of interleaved practice of motor skills is associated with changes in functional brain network topology that differ between younger and older adults. *Neurobiology of aging*, *42*, 189-198.

Luna, B., Marek, S., Larsen, B., Tervo-Clemmens, B., & Chahal, R. (2015). An integrative model of the maturation of cognitive control. *Annual review of neuroscience*, *38*, 151-170.

Marek, S., Hwang, K., Foran, W., Hallquist, M. N., & Luna, B. (2015). The contribution of network organization and integration to the development of cognitive control. *PLoS Biology*, *13*(12), e1002328.

Miraglia, F., Vecchio, F., & Rossini, P. M. (2018). Brain electroencephalographic segregation as a biomarker of learning. *Neural Networks*, *106*, 168-174.

Morgan, S. E., White, S. R., Bullmore, E. T., & Vértes, P. E. (2018). A network neuroscience approach to typical and atypical brain development. *Biological Psychiatry: Cognitive Neuroscience and Neuroimaging*. *3(9)*, 754-766.

Nie, J., Li, G., & Shen, D. (2013). Development of cortical anatomical properties from early childhood to early adulthood. *NeuroImage*, *76*, 216–224.

Nie, J., Li, G., Wang, L., Shi, F., Lin, W., Gilmore, J. H., & Shen, D. (2014). Longitudinal development of cortical thickness, folding, and fiber density networks in the first 2 years of life. *Human Brain Mapping*, *35*(8), 3726–3737.

Petanjek, Z., Judaš, M., Šimić, G., Rašin, M. R., Uylings, H. B., Rakic, P., & Kostović, I. (2011). Extraordinary neoteny of synaptic spines in the human prefrontal cortex. *Proceedings of the National Academy of Sciences*, *108*(32), 13281-13286.

Robertson, E. M. (2007). The serial reaction time task: implicit motor skill learning?. *Journal of Neuroscience*, *27*(38), 10073-10075.

Roussotte, F. F., Bramen, J. E., Nunez, S. C., Quandt, L. C., Smith, L., O'Connor, M. J., Bookheimer, S.Y., & Sowell, E. R. (2011). Abnormal brain activation during working memory in children with prenatal exposure to drugs of abuse: the effects of methamphetamine, alcohol, and polydrug exposure. *Neuroimage*, *54*(4), 3067-3075.

Rubinov, M., & Sporns, O. (2010). Complex network measures of brain connectivity: uses and interpretations. *Neuroimage*, *52*(3), 1059-1069.

Satterthwaite, T. D., Wolf, D. H., Ruparel, K., Erus, G., Elliott, M. A., Eickhoff, S. B., Gennatas, E.D., Jackson, C., Prabhakaran, K., Smith, A., & Hakonarson, H. (2013). Heterogeneous impact of motion on fundamental patterns of developmental changes in functional connectivity during youth. *Neuroimage*, *83*, 45-57.

Schleepen, T. M., & Jonkman, L. M. (2009). The development of non-spatial working memory capacity during childhood and adolescence and the role of interference control: an N-Back task study. *Developmental neuropsychology*, *35*(1), 37-56.

Shen, D., & Davatzikos, C. (2002). HAMMER: hierarchical attribute matching mechanism for elastic registration. *IEEE transactions on medical imaging*, *21*(11), 1421-1439.

Shi, F., Fan, Y., Tang, S., Gilmore, J. H., Lin, W., & Shen, D. (2010). Neonatal brain image segmentation in longitudinal MRI studies. *Neuroimage*, *49*(1), 391-400.

Shi, F., Wang, L., Dai, Y., Gilmore, J. H., Lin, W., & Shen, D. (2012). LABEL: pediatric brain extraction using learning-based meta-algorithm. *Neuroimage*, *62*(3), 1975-1986.

Shine, J. M., & Poldrack, R. A. (2018). Principles of dynamic network reconfiguration across diverse brain states. *NeuroImage*, *180*, 396-405.

Sled, J. G., Zijdenbos, A. P., & Evans, A. C. (1998). A nonparametric method for automatic correction of intensity nonuniformity in MRI data. *IEEE transactions on medical imaging*, *17*(1), 87-97.

Smith, S., Duff, E., Groves, A., Nichols, T. E., Jbabdi, S., Westlye, L. T., Tamnes, C.K., Engvig, A., Walhovd, K.B., Fjell, A.M., & Johansen-Berg, H. (2019). Structural variability in the

human brain reflects fine-grained functional architecture at the population level. *Journal of Neuroscience*, *39*(31), 6136-6149.

Smith, S. M., Fox, P. T., Miller, K. L., Glahn, D. C., Fox, P. M., Mackay, C. E., Filippini, N., Watkins, K.E., Toro, R., Laird, A.R., & Beckmann, C. F. (2009). Correspondence of the brain's functional architecture during activation and rest. *Proceedings of the National Academy of Sciences*, *106*(31), 13040-13045.

Smith, S. M., Jenkinson, M., Woolrich, M. W., Beckmann, C. F., Behrens, T. E., Johansen-Berg, H., Bannister, P.R., De Luca, M., Drobnjak, I., Flitney, D.E., & Niazy, R. K. (2004). Advances in functional and structural MR image analysis and implementation as FSL. *Neuroimage*, *23*, S208-S219.

Sporns, O. (2013). Network attributes for segregation and integration in the human brain. *Current opinion in neurobiology*, *23*(2), 162-171.

Stollstorff, M., Foss-Feig, J., Cook Jr, E. H., Stein, M. A., Gaillard, W. D., & Vaidya, C. J. (2010). Neural response to working memory load varies by dopamine transporter genotype in children. *Neuroimage*, *53*(3), 970-977.

Thomas, K. M., Hunt, R. H., Vizueta, N., Sommer, T., Durston, S., Yang, Y., & Worden, M. S. (2004). Evidence of developmental differences in implicit sequence learning: an fMRI study of children and adults. *Journal of cognitive neuroscience*, *16*(8), 1339-1351.

Thomas, K. M., & Nelson, C. A. (2001). Serial reaction time learning in preschool-and school-age children. *Journal of experimental child psychology*, *79*(4), 364-387.

Wang, L., Shi, F., Yap, P. T., Gilmore, J. H., Lin, W., & Shen, D. (2012). 4D multi-modality tissue segmentation of serial infant images. *PloS one*, *7*(9), e44596.

Yeo, B. T., Krienen, F. M., Sepulcre, J., Sabuncu, M. R., Lashkari, D., Hollinshead, M., Roffman, J.L., Smoller, J.W., Zöllei, L., Polimeni, J.R., & Fischl, B. (2011). The organization of the human cerebral cortex estimated by intrinsic functional connectivity. *Journal of Neurophysiology*, *106*(3), 1125-1165.

Yeo, B. T., Sabuncu, M. R., Vercauteren, T., Ayache, N., Fischl, B., & Golland, P. (2010). Spherical demons: fast diffeomorphic landmark-free surface registration. *IEEE transactions on medical imaging*, *29*(3), 650-668.

Zhao, T., Xu, Y., & He, Y. (2019). Graph theoretical modeling of baby brain networks. *NeuroImage*, *185*, 711-727.